Engineering Structures 298 (2024) 117025

Contents lists available at ScienceDirect

Engineering Structures

journal homepage: www.elsevier.com/locate/engstruct

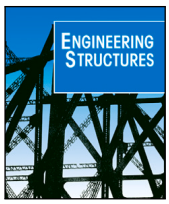

Generalised analytical solutions for linear and non-linear bond–slip models for externally bonded FRP to a concrete substrate

Levingshan Augusthus Nelson [a,*], Laurence Weekes [a], Gabriele Milani [b], Mustafa Al-Allaf [c]

[a] School of Science, Engineering and Environment, University of Salford, United Kingdom
[b] Department of Architecture, Built environment and Construction engineering, Technical University in Milan, Italy
[c] Department of Civil Engineering, Al-Nahrain University, Iraq

ARTICLE INFO

Keywords:
Bond–slip model
Epoxy-bonded FRP
Retrofitting of concrete

ABSTRACT

This article presents a set of novel analytical derivations from generalised bond–slip models using first principles, which can be used to predict experimental outcomes, including maximum load resistance, load-slip response, and strain throughout the bonded length. The generalised bond–slip models are constructed in a way that can be translated into various shapes, including linear, nonlinear and exponential forms, all of which have been used in the literature to explain the bond–slip behaviour of epoxy-bonded FRP on concrete. When the prerequisites for the derivations are satisfied, as demonstrated in this paper, a comprehensive validation of a bond–slip model is possible. Furthermore, the transformability of the generalised bond–slip models and the analytical nature of the derivations also allowed for the comparison of several bond–slip models simultaneously.

1. Introduction

The retrofitting of damaged civil engineering structures is the most economical, social and environmental solution compared to reconstruction [1]. The retrofitting of structures varies depending on the type of defective structure, the retrofitting materials used, and the current understanding of retrofitting techniques [2]. Of various retrofitting materials, fibre reinforced polymers (FRP) are widely used due to their high strength-to-weight ratio and resistance to corrosion [3]. FRPs have been used in several ways: epoxy-bonded external FRP sheets [3], near-surface mounted FRP bars [4] and post-tensioned FRP straps [5]. Of these, an epoxy-bonded FRP sheet is preferred as it is less intrusive and retrofitting of the structures may be carried out while the structure is in service [1].

To understand the effectiveness and interaction of FRP, various types of experimental investigations, such as single and double shear-lap tests, have been carried out [6–9]. In addition, numerous strength-based models [10,11] and bond–slip models [12–14] have been proposed to demonstrate the behaviour observed during the experimental bond tests.

Strength-based models are based on the mechanical and geometrical properties of the test samples, which directly offer bond (load) resistance. Therefore, they are often preferred in the design environment. However, the interface behaviour between the epoxy-bonded FRP and concrete may not be achievable through strength-based models. In contrast, bond–slip models, which are essential in constitutive modelling, were developed using the interface bond and material properties of FRP, concrete and epoxy glue [15–17].

In the early stage of development of bond–slip models, the main outputs of the experimental tests were the maximum bond (load) resistance and the load-slip curves [11]. Using these outputs, the interfacial bond properties for a given shape were back-calculated because these cannot be directly obtained from the experimental results. Therefore, the validations of the bond–slip models were achieved by developing empirical mathematical formulae or by incorporating the bond–slip models within the finite element analysis.

Later, an approximate strain profile along the FRP using electronic resistance strain gauge measurements at discrete locations was established. A continuous strain profile along the FRP was recently developed using image processing techniques such as digital image correlation (DIC) [18,19]. For several samples tested, upper and lower bounds of strain profiles were generated. A range of interfacial bond stress vs slip profiles (within the upper and lower bounds of stress) was developed using the range of the strain profile, as shown in Fig. 1. Approximate best-fit lines were considered to generate the mathematical equations for the ascending and descending curves of the bond–slip models. Therefore, the number of possible bond–slip models depends on the method used for the best fit and the shape considered

* Corresponding author.
E-mail address: l.augusthusnelson@salford.ac.uk (L. Augusthus Nelson).

https://doi.org/10.1016/j.engstruct.2023.117025
Received 13 March 2023; Received in revised form 28 September 2023; Accepted 6 October 2023
Available online 19 October 2023

by the researchers. For illustration purposes, Fig. 1 shows two different possible bond–slip models. The possible best-fit bond–slip models were extended due to variability in material properties, workmanship during the installation of the FRP, environmental conditions, and nature and repeatability of the loading conditions. Thus, numerous bond–slip models have been established in the literature at present.

To calibrate a chosen bond–slip model, researchers often used semi-empirical mathematical formulae or finite element analysis. The main drawback of the semi-empirical mathematical formulae was that it was calibrated for a specific set of experimental test results, and the model needed to be recalibrated when a new set of experimental results became available. Furthermore, even though finite element (FE) analysis provides better visualisation of output, creating and debugging the models requires a good understanding of the software package used. In addition, the modelling of the test samples in the FE package take a substantial amount of time as the variation in test samples should be considered individually.

For these reasons, theoretical derivations to predict the behaviour of the test samples were derived from bond–slip models. Wu et al. [20] used a single mathematical bond–slip formula (which represents ascending and descending curves) to derive analytical solutions. However, most of the proposed bond–slip models in the literature have two separate mathematical functions (each defining the ascending and descending curves of the bond–slip models separately), and thus the analytical solutions of Wu et al. could not be extended. Hence, Augusthus Nelson et al. [21] derived analytical solutions for a bond–slip model with nonlinearly ascending (possible to converge to linear form) and linear descending curves. However, another most common form of the bond–slip model is the non-linearly ascending and exponentially descending curves, which have been the focus of this current work.

Post-processing of the experimental findings conducted by Mazzotti et al. [22] reveals that certain test specimens exhibit an exponentially softening (descending) bond–slip curve. In a related context, Lu et al. [23] have contributed significantly to the discourse by introducing three distinct bond–slip models, each designed to emphasise the pivotal role of bond–slip curve configuration. It was observed that two of these models exhibit exponential softening characteristics in their bond–slip curves, while the third features a bi-linear model encompassing both ascending and descending curves. Furthermore, Lu et al. have explored predictive capabilities using semi-empirical derivations of these three bond–slip models concerning experimental attributes, demonstrating that differences in the softening curves can result in variances in the projected load-bearing capacity and deformation response. It is noteworthy that Lu et al. also showed that bond–slip models characterised by exponential softening patterns yield superior predictions when compared to alternative models. It should also be noted that the studies suggested that the predictions of the effective bond length change significantly between the shape of the bond–slip model [23,24]. At the same time, it has little impact on the maximum load resistance. These observations could not be confirmed as experimental predictions using various shapes of bond–slip models are unified (due to the use of empirical constants) [25,26]. Hence, the primary objective of this paper is to develop theoretical derivations for predicting experimental characteristics without the reliance on empirical constants, in order to facilitate the concurrent comparison of multiple bond–slip models. Specifically, this study focuses on the theoretical formulation for forecasting experimental attributes using the non-linearly ascending and exponentially descending bond–slip model. Another motivation for the current work is to demonstrate that these unique theoretical derivations (solutions) can be used to establish the complete interaction behaviour (such as bond resistance, load–deformation curves, stress and strain profiles along the FRP and concrete) for most of the bond–slip models available in the literature.

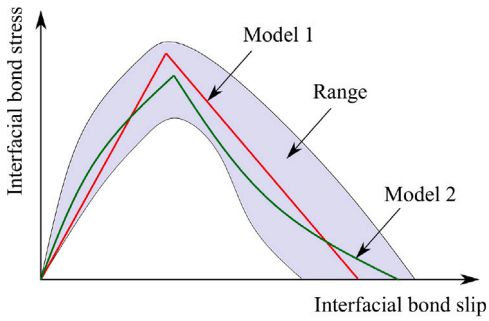

Fig. 1. Range of bond stresses and slip at the interface with possible bond–slip models.

2. Generalised bond–slip models and their theoretical derivation

In the literature, when it comes to epoxy-bonded FRP on a concrete surface, most bond–slip models have two separate curves (a mathematical equation defines each curve): ascending and descending. The shapes of the ascending and descending curves vary between linear, curvilinear, and exponential. Recently, Augusthus Nelson et al. [21] derived a complete and comprehensive analytical solutions for a generalised bond–slip model with ascending non-linear power curve and descending linear curve (see Fig. 2(a)), given as:

$$\tau = \begin{cases} \tau_{max}\left(\frac{s}{s_1}\right)^{\alpha} & 0 \le s \le s_1 \\ \tau_{max}\left(\frac{s_2 - s}{s_2 - s_1}\right) & s_1 \le s \le s_2 \\ 0 & s_2 \le s \end{cases} \tag{1}$$

where s_1 and s_2 are the slip values that demonstrate each region of behaviour, τ_{max} is the maximum bond stress, and α is a constant that defines the nonlinear ascending curve of the bond–slip model (Fig. 2(a)).

The main advantage of this generalised bond–slip model is that it can be transformed into various bond–slip models proposed by [23,27–31], hence, the analytical solutions derived by Augusthus Nelson et al. too can be easily transformed for any of these models proposed in the literature. This approach allows the validation of any of these models to be performed without time-consuming finite element methods or any unnecessary semi-empirical solutions. It should be noted that the transformability of the solutions derived by Augusthus Nelson et al. [21] is limited to a bond–slip model with a linear descending curve. However, few other bond–slip models in the literature have an exponentially descending curve [16,23,32,33] (see Fig. 2(b)). To expand this analytical approach, the focus of this current work is to derive analytical solutions for a bond–slip model with an ascending power curve and a descending exponential curve (see Fig. 2(b)), can be given as:

$$\tau = \begin{cases} \tau_{max}\left(\frac{s}{s_1}\right)^{\alpha} & 0 \le s \le s_1 \\ \tau_{max} e^{-\beta(s - s_1)} & s_1 \le s \end{cases} \tag{2}$$

where s_1 is the slip corresponding to the maximum bond stress τ_{max}, and α and β are the constants that define the nonlinear ascending and descending curves of the bond stress–slip model (Fig. 2(b)).

In both cases, the mathematical function of the ascending curve is the same. Hence, mathematical derivations for the ascending curve are briefly summarised here (comprehensive derivations can be found in Augusthus Nelson et al. [21]). However, complete derivations for the descending exponential curve are presented in this paper. Also, here onwards, the analytical model presented in Augusthus Nelson et al. [21] is referred to as Generalised Bond–slip Model 1. The model presented in this paper is referred to as Generalised Bond–slip Model 2.

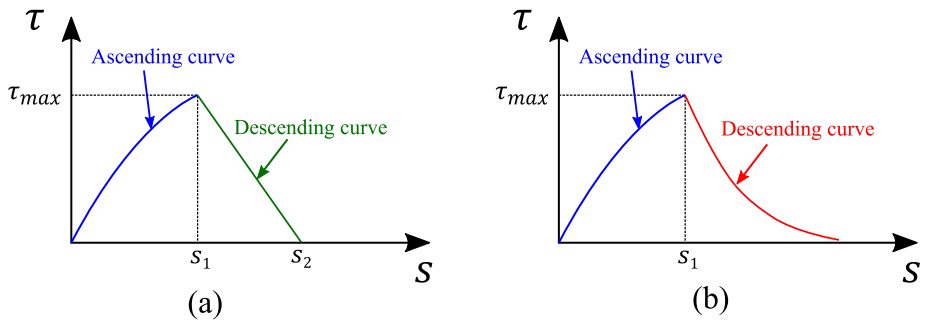

Fig. 2. Generalised Bond–slip Models (a) Generalised Bond–slip Model 1: nonlinearly ascending and linearly descending curves (mathematical formulae are in Eq. (1)), and (b) Generalised Bond–slip Model 2: nonlinearly ascending and exponentially descending curves (mathematical formulae are in Eq. (2)).

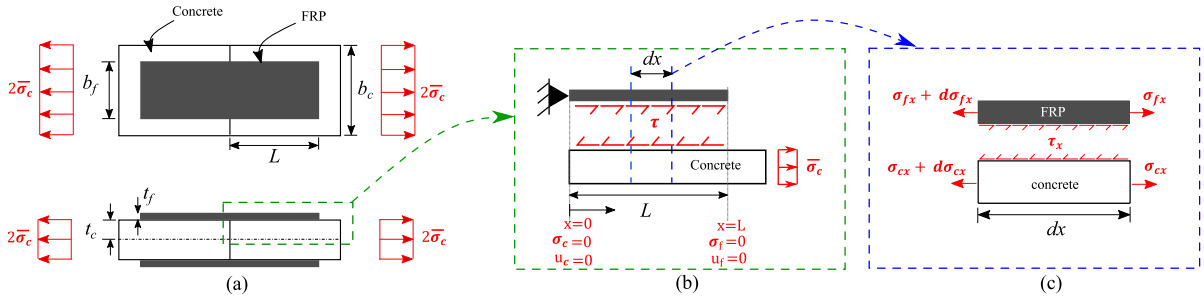

Fig. 3. (a) Double-lap shear test sample with dimensions, (b) idealisation to single lap shear and shearing between FRP and concrete, and (c) differential segment of bonded joint.

2.1. Governing equation

The resultant slip between FRP and the concrete substrate along the FRP is defined as [12,20,34]:

$$s = u_f - u_c \tag{3}$$

Second order derivation can be given as:

$$\frac{\mathrm{d}^2 s}{\mathrm{d}x^2} = \frac{\mathrm{d}^2 u_f}{\mathrm{d}x^2} - \frac{\mathrm{d}^2 u_c}{\mathrm{d}x^2} \tag{4}$$

where s is the slip; u_f and u_c are the displacement of the FRP and the concrete, respectively. The governing equation was initially derived for a double-lap shear test sample (Fig. 3(a)), which is then idealised for single shear (Fig. 3(b)). The differential segment was then considered to develop equilibrium conditions, as seen in Fig. 3(c). The equilibrium conditions give:

$$\begin{aligned} b_c t_c \frac{\mathrm{d}\sigma_c}{\mathrm{d}x} + \tau b_f = 0 \\ b_f t_f \frac{\mathrm{d}\sigma_f}{\mathrm{d}x} - \tau b_f = 0 \end{aligned} \tag{5}$$

However,

$$\begin{aligned} \frac{\mathrm{d}\sigma_c}{\mathrm{d}x} = E_c \frac{\mathrm{d}^2 u_c}{\mathrm{d}x^2} \\ \frac{\mathrm{d}\sigma_f}{\mathrm{d}x} = E_f \frac{\mathrm{d}^2 u_f}{\mathrm{d}x^2} \end{aligned} \tag{6}$$

It should be noted that the current derivation considers the concrete to be elastic and does not consider the rupture of concrete or the FRP. Therefore, the derivations presented by the equilibrium and compatibility conditions only apply to the bond failure between concrete and FRP (in the epoxy glue). Experimental results in the literature support the slip between concrete and FRP, for which concrete is in an elastic condition. Thus, Yuan et al. [12] and Wu et al. [20,34] have used the equilibrium and compatibility conditions, as shown in Eq. (7). By combining Eqs. (5) and (6), equilibrium conditions give:

$$\begin{aligned} \frac{\mathrm{d}^2 u_c}{\mathrm{d}x^2} + \frac{b_f}{E_c t_c b_c}\tau = 0 \\ \frac{\mathrm{d}^2 u_f}{\mathrm{d}x^2} - \frac{b_f}{E_f t_f b_f}\tau = 0 \end{aligned} \tag{7}$$

Equating Eqs. (7) and Eq. (4) results in:

$$\frac{\mathrm{d}^2 s}{\mathrm{d}x^2} = K\tau \tag{8}$$

where

$$K = \frac{E_c t_c b_c + E_f t_f b_f}{E_f t_f E_c t_c b_c} \tag{9}$$

The extended version of the derivation is presented in Augusthus Nelson et al. [21]. It is also shown that the K of the single-lap shear test can deduced to:

$$K = \frac{1}{E_f t_f} \tag{10}$$

where σ_c, E_c, t_c and ϵ_c are axial stress, Young's modulus of elasticity, the thickness of half the concrete prism and the strain of concrete, respectively. Moreover, σ_f, E_f, t_f, and ϵ_f are the axial stress, Young's modulus of elasticity, and the deformation throughout the thickness of the FRP reinforcement, respectively. The governing equation, Eq. (8), is general and can be used for any bond–slip relationship, which can be applied for each segment representing a particular bond–slip ($\tau - s$) relation.

However, at least two boundary conditions are needed to solve a second-order differential equation. The following boundary conditions can be established based on the stress and strain experienced by the FRP and concrete, as depicted in Fig. 3(b).

$$\begin{aligned} u_f = 0 \quad &\text{at} \quad x = 0 \\ \sigma_f = E_f \frac{\mathrm{d}u_f}{\mathrm{d}x} = 0 \quad &\text{at} \quad x = L \\ \sigma_c = E_c \frac{\mathrm{d}u_c}{\mathrm{d}x} = 0 \quad &\text{at} \quad x = 0 \\ \sigma_c = E_c \frac{\mathrm{d}u_f}{\mathrm{d}x} = \bar{\sigma_c} \quad &\text{at} \quad x = L \end{aligned} \tag{11}$$

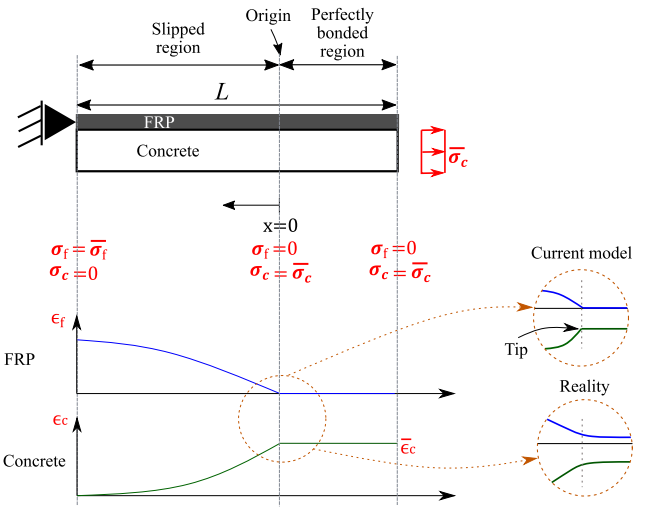

Fig. 4. Transformation of origin corresponds to bond stress and slip, and model representation against reality.

These boundary conditions, however, are not directly applicable to Eq. (8). Therefore, boundary conditions that correspond to bond stress and slip need to be established to solve the governing Eq. (8). The generalised bond–slip models presented by Eqs. (1) and (2) are for the bond stress and slip, in which bond stress is zero and where there is no slip. Therefore, the origin of x is taken where there is no slip (as shown in Fig. 4), which forms the first boundary condition. Additionally, it is hypothesised that the rate of change in the slip at the origin is zero, which forms the second boundary condition. Therefore, both boundary conditions can be given as follows:

$$\begin{aligned} s &= 0 \quad \text{at} \quad x = 0 \\ \frac{\mathrm{d}s}{\mathrm{d}x} &= 0 \quad \text{at} \quad x = 0 \end{aligned} \tag{12}$$

It should be observed that the origin of $x(=0)$ shifts towards to unloaded bond end (where there is axial stress on the concrete) with increasing applied load, as illustrated in Fig. 5. This is maintained for the remainder of the derivation. In addition, the ascending curve area and the primary zone convey the same notion: similar to the secondary zone and area with descending curves. These were used interchangeably to improve readability.

2.2. Primary zone (ascending bond–slip region)

For both Generalised Models (Eqs. (1) and (2)), the ascending curves have the same mathematical expressions. In addition, the primary zone is activated when the slip between FRP and concrete occurs ($s \leq s_1$) as shown in Fig. 5(b). The bond stress in the primary zone is defined as:

$$\tau_p = \tau_{max} \left(\frac{s}{s_1} \right)^{\alpha} \tag{13}$$

Therefore the governing Eq. (8) for the primary zone can be given as:

$$\frac{\mathrm{d}^2 s}{\mathrm{d}x^2} = K \tau_{max} \left(\frac{s}{s_1} \right)^{\alpha} \tag{14}$$

This second order differential equation can be solved using the boundary conditions presented in Eqs. (12). The complete mathematical derivation of the primary zone was presented in Augusthus Nelson et al. [21]. Here, a summary of the derivations is presented to provide context. The slip along the bonded length x can be given as:

$$s = \left(\frac{K\rho_1 (1-\alpha)^2}{2(1+\alpha)} \right)^{\frac{1}{1-\alpha}} x^{\frac{2}{1-\alpha}} \tag{15}$$

where K is the constant for an experimental setup, $\rho_1 = \frac{\tau_{max}}{s_1^{\alpha}}$ and α has a positive value (according to most existing bond–slip models, $0 \leq \alpha \leq 1$). The length of the primary zone along the FRP (l_1) can be given as:

$$l_1 = \left(\frac{2(1+\alpha)}{K\rho_1 (1-\alpha)^2} \right)^{\frac{1}{2}} s_1^{\frac{1-\alpha}{2}} \tag{16}$$

Furthermore, the bond stress along the FRP reinforcement at a distance x can be given as:

$$\tau_p = \rho_1 \left(\frac{K\rho_1 (1-\alpha)^2}{2(1+\alpha)} \right)^{\frac{\alpha}{1-\alpha}} x^{\frac{2\alpha}{1-\alpha}} \tag{17}$$

The maximum load resistance of the primary zone can be given as:

$$F_{p,max} = b_f \rho_1 \left(\frac{K\rho_1 (1-\alpha)^2}{2(1+\alpha)} \right)^{\frac{\alpha}{1-\alpha}} l_1^{\frac{1+\alpha}{1-\alpha}} \tag{18}$$

The FRP strain distribution along the length in the primary zone can be given as:

$$\epsilon_f = \frac{1}{E_f t_f} \int_0^x \tau_p dx = \frac{F_p}{t_f b_f E_f} \tag{19}$$

Based on the bond–slip model considered for this derivation, the bond stress and strain distributions along with the reinforcement and load-slip curve can be obtained if the parameters s_1 and α are known for double or single shear tests.

2.3. Primary (ascending) and secondary (descending) zones

The secondary zone is activated when the slip between the FRP and concrete exceeds s_1, as shown in Fig. 5(c). The primary zone remains and moves along towards the unloaded end (See Fig. 5(d)). The maximum primary zone length from Eq. (15) can be given as:

$$l_1 = \left(\frac{2(1+\alpha)}{K\rho_1 (1-\alpha)^2} \right)^{\frac{1}{2}} s_1^{\frac{1-\alpha}{2}} \tag{20}$$

At the end of primary zone (boundary between the primary zone and the secondary zone), the first-order differentiation of Eq. (15) can be given as:

$$\left(\frac{\mathrm{d}s}{\mathrm{d}x} \right)_{l_1} = \left(\frac{2K\rho_1}{1+\alpha} \right)^{\frac{1}{2}} s_1^{\frac{1+\alpha}{2}} \tag{21}$$

As illustrated in Fig. 5, the origin for the slip moves towards the unloaded end. However, to derive and obtain the solutions for this second-order non-linear differential equation, bond length corresponds to the secondary zone (descending curve) is denoted as xx as shown in Fig. 5(d). The bond length is then revised to acquire the affected length from the primary zone origin after the solution has been found. The stress–slip bond model for the secondary zone can be given by (Eq. (2)):

$$\tau_s = \tau_{max} e^{-\beta(s-s_1)} \tag{22}$$

Substituting Eq. (22) into Eq. (8) gives:

$$\frac{\mathrm{d}^2 s}{\mathrm{d}xx^2} = K \tau_{max} e^{-\beta(s-s_1)} \tag{23}$$

By integrating both sides of the equation, the following can be given as:

$$\frac{1}{\beta} e^{\beta(s-s_1)} \frac{\mathrm{d}s}{\mathrm{d}xx} = K \tau_{max} xx + C_1 \tag{24}$$

and,

$$\frac{1}{\beta^2} e^{\beta(s-s_1)} = K \tau_{max} \frac{xx^2}{2} + C_1 xx + C_2 \tag{25}$$

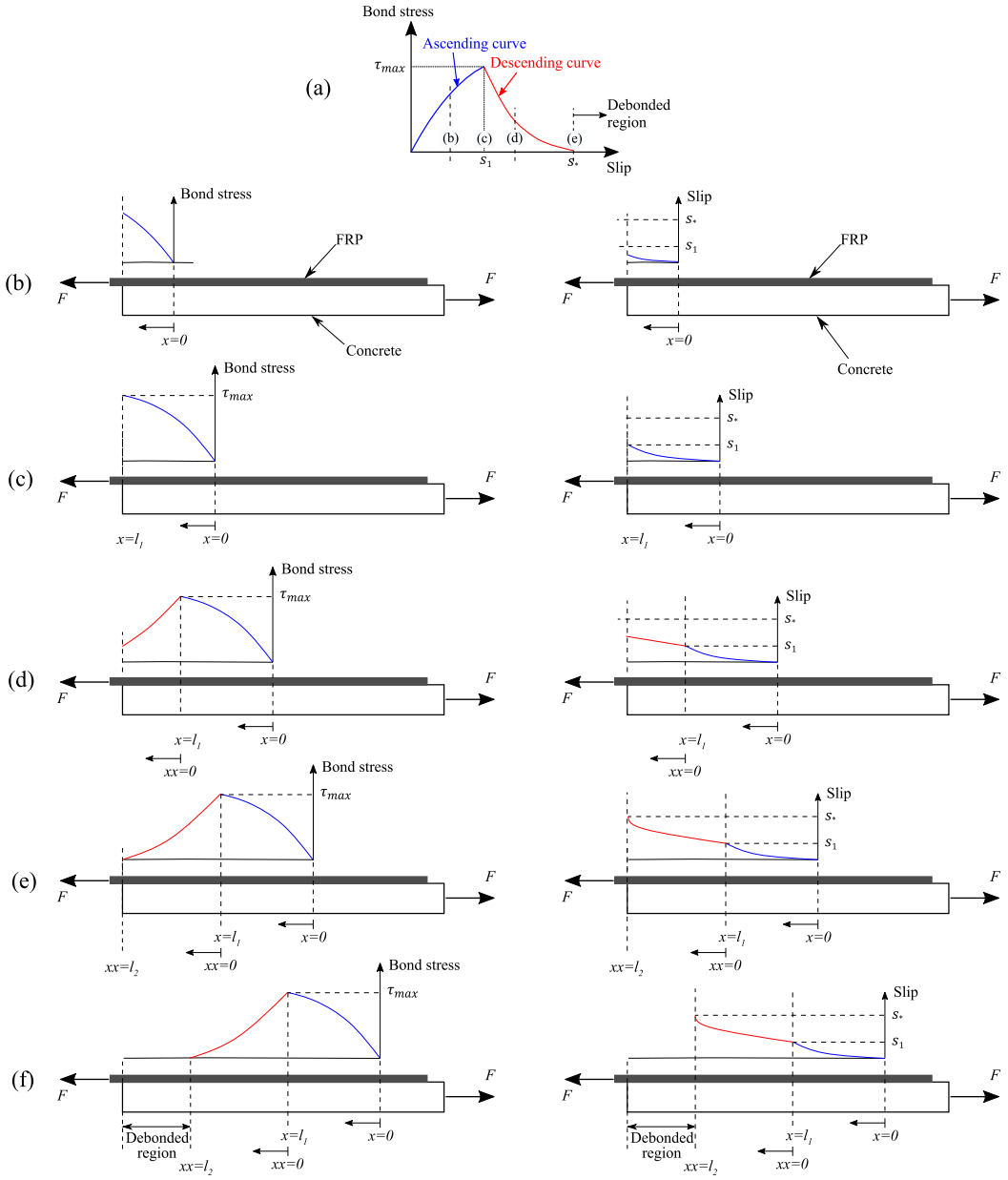

Fig. 5. Bond stress and slip development along the bonded length are illustrated at various stages: (a) Bond–slip model (s_* is s_2 for Generalised Model 1 and s_γ for Generalised Model 2 (See Fig. 6)); (b) partial development of the ascending curve; (c) full development of the ascending curve; (d) fully developed ascending curve and partial development of the descending curve; (e) fully developed ascending and descending curves; (f) with increasing applied load, fully developed ascending and descending curves move towards the unloaded end.

where, C_1 and C_2 are constants. It should be noted that the local distance along the FRP for the secondary zone is denoted by xx compared to the global distance x. Therefore, $x = l_1$ for $xx = 0$.

Eqs. (24) and (25) for the secondary zone are required to comply with the equilibrium and compatibility conditions. Therefore, s and $\frac{ds}{dx}$ (Eqs. (20) and (21)) at the end of the primary zone can be used as boundary conditions in Eqs. (24) and (25), which leads to:

$$C_1 = \frac{1}{\beta}\left(\frac{2K\rho_1}{(1+\alpha)}\right)^{\frac{1}{2}} s_1^{\frac{1+\alpha}{2}} \tag{26}$$

and,

$$C_2 = \frac{1}{\beta^2} \tag{27}$$

Constants C_1 and C_2 depend on the characteristic of the proposed bond–slip model. Therefore, the bond stress in the secondary zone can be given as:

$$\tau_s = \frac{\tau_{max}}{\beta^2 K \tau_{max}\frac{xx^2}{2} + \beta^2 C_1 xx + 1} \tag{28}$$

The descending exponential curve reaches zero stress at the infinite length of the FRP. According to this mathematical model, the tail part of the exponential curve does not contribute significantly to the load carrying capacity. Therefore, to obtain the effective bond length and load-carrying capacity of the system, a ratio between cut-off stress (τ_γ) and maximum bond stress (τ_{max}) can be considered as (see Fig. 6):

$$\gamma = \frac{\tau_\gamma}{\tau_{max}} \leq 1 \tag{29}$$

Therefore, Eq. (22) at the cutoff point with the corresponding slip s_γ, where the bond considered failed, can be given as:

$$\frac{\tau_\gamma}{\tau_{max}} = \gamma = e^{-\beta(s_\gamma - s_1)} \tag{30}$$

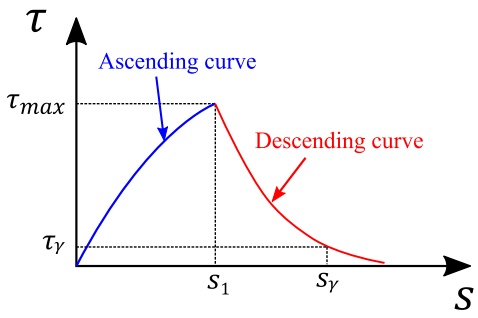

Fig. 6. Generalised bond–slip Model 2 with the limiting stress and corresponding slip.

Eq. (25) at the end of the secondary zone (l_2), can be given as:

$$\frac{1}{\beta^2}e^{\beta(s_\gamma - s_1)} = K\tau_{max}\frac{l_2^2}{2} + C_1 l_2 + C_2 \tag{31}$$

C_1, C_2 and $e^{\beta(s_\gamma - s_1)}$ can be replaced using Eqs. (26), (27) and (30), respectively.

$$\frac{1}{\beta^2\gamma} = K\tau_{max}\frac{l_2^2}{2} + \frac{1}{\beta}\left(\frac{2K\rho_1}{(1+\alpha)}\right)^{\frac{1}{2}} s_1^{\frac{1+\alpha}{2}} l_2 + \frac{1}{\beta^2} \tag{32}$$

It can be reduced to a quadratic equation:

$$\frac{\beta^2\gamma K\tau_{max}}{2}l_2^2 + \beta\gamma\left(\frac{2K\rho_1}{(1+\alpha)}\right)^{\frac{1}{2}} s_1^{\frac{1+\alpha}{2}} l_2 + (\gamma - 1) = 0 \tag{33}$$

where l_2 is the unknown. The length of the secondary zone (l_2) must be positive and real. Therefore, the discriminant must be greater than or equal to zero, which can be given as:

$$2K\beta^2\gamma\tau_{max}\left(\frac{\gamma s_1 + (1-\gamma)(1+\alpha)}{(1+\alpha)}\right) \geq 0 \tag{34}$$

In this equation, $1-\gamma$ is positive as $0 \leq \gamma \leq 1$ and rest of the parameters are positive. Therefore, solutions of Eq. (33) will be real numbers. However, l_2 is distance measurement and cannot be negative. Therefore, the length associated with the fully developed secondary zone can be given as:

$$l_2 = \left(\frac{2}{\beta^2\gamma K\tau_{max}(1+\alpha)}\right)^{\frac{1}{2}}\left(\left(\gamma s_1 + (1+\alpha)(1-\gamma)\right)^{\frac{1}{2}} - (\gamma s_1)^{\frac{1}{2}}\right) \tag{35}$$

Hence, the effective length can be given using Eqs. (20) and (35) as:

$$l_e = l_1 + l_2 = \left(\frac{2(1+\alpha)}{K\rho_1(1-\alpha)^2}\right)^{\frac{1}{2}} s_1^{\frac{1-\alpha}{2}} + \left(\frac{2}{\beta^2\gamma K\tau_{max}(1+\alpha)}\right)^{\frac{1}{2}} \times \left(\left(\gamma s_1 + (1+\alpha)(1-\gamma)\right)^{\frac{1}{2}} - (\gamma s_1)^{\frac{1}{2}}\right) \tag{36}$$

The secondary zone force can be obtained by integrating the stress function with respect to xx with the width of the FRP sheet, which can be given as (rearranged from Eq. (25)):

$$F_s = b_f\int_0^{xx}\tau_s dxx = b_f\tau_{max}\int_0^{xx}\frac{1}{\beta^2 K\tau_{max}\frac{xx^2}{2} + \beta^2 C_1 xx + 1}dxx \tag{37}$$

Eq. (37) can be re-arranged to:

$$F_s = \frac{2b_f}{\beta^2 K}\int_0^{xx}\frac{1}{xx^2 + \frac{2C_1}{K\tau_{max}}xx + \frac{2}{\beta^2 K\tau_{max}}}dxx \tag{38}$$

$$F_s = \frac{2b_f}{\beta^2 K}\int_0^{xx}\frac{1}{xx^2 + Pxx + Q}dxx \tag{39}$$

where, $P = \frac{2C_1}{K\tau_{max}}$ and $Q = \frac{2}{\beta^2 K\tau_{max}}$, which are constant for specific bond–slip model. The integration of the inverse quadratic equation can be rearranged as:

$$F_s = \frac{2b_f}{\beta^2 K}\frac{1}{\sqrt{\frac{4Q-P^2}{4}}}\int_0^{xx}\frac{\frac{1}{\sqrt{\frac{4Q-P^2}{4}}}}{\left(\frac{xx+\frac{P}{2}}{\sqrt{\frac{4Q-P^2}{4}}}\right)^2 + 1}dxx \tag{40}$$

The integration part has $\int\frac{1}{u^2+1}du = \arctan(u) + C$ format. Hence, the force due to the secondary zone can be given as:

$$F_s = \frac{4b_f}{\beta^2 K\sqrt{4Q-P^2}}\left(\arctan\left(\frac{xx+\frac{P}{2}}{\sqrt{\frac{4Q-p^2}{4}}}\right) + C\right)\Big|_0^{xx} \tag{41}$$

By applying the limiting values, the force due to the secondary zone can be given as:

$$F_s = \frac{4b_f}{\beta^2 K\sqrt{4Q-P^2}}\left(\arctan\left(\frac{xx+\frac{P}{2}}{\sqrt{\frac{4Q-p^2}{4}}}\right) - \arctan\left(\frac{\frac{P}{2}}{\sqrt{\frac{4Q-p^2}{4}}}\right)\right) \tag{42}$$

For the fully developed secondary zone ($xx = l_2$) (Eq. (35)), the maximum force can be given as:

$$F_{s,max} = \frac{4b_f}{\beta^2 K\sqrt{4Q-P^2}}\left(\arctan\left(\frac{l_2+\frac{P}{2}}{\sqrt{\frac{4Q-p^2}{4}}}\right) - \arctan\left(\frac{\frac{P}{2}}{\sqrt{\frac{4Q-p^2}{4}}}\right)\right) \tag{43}$$

The maximum debonding load can be obtained by adding Eqs. (18) and (43):

$$F_{max} = F_{p,max} + F_{s,max} \tag{44}$$

The FRP strain in the secondary zone can be obtained as:

$$\epsilon_f = \frac{1}{E_f t_f}\int_0^{l_1}\tau_p dx + \frac{1}{E_f t_f}\int_{l_1}^{x}\tau_s dx = \frac{F_{p,max}}{t_f b_f E_f} + \frac{F_s}{t_f b_f E_f} \tag{45}$$

Therefore, the maximum FRP strain can be obtained as:

$$\epsilon_{f,max} = \frac{F_{p,max}}{t_f b_f E_f} + \frac{F_{s,max}}{t_f b_f E_f} = \frac{F_{max}}{t_f b_f E_f} \tag{46}$$

3. Summary of theoretical derivations and transform-ability

The theoretical derivations presented by Augusthus Nelson et al. [21] and in the present work can be used to elaborate the complete stress–strain relationship, the load–deformation relationship, the maximum bond (load) resistance, and the effective length of the bonded FRP of a test sample. However, in this section, the effective bond length and the ultimate bond resistance (load resistance capacity) are summarised in Table 1. The effective length of the bond and the ultimate resistance to the bond depend on the geometry of the test samples and the experimental setup (which are given by the parameter K) and the bond–slip parameters (interfacial bond properties). As shown in Table 1, the formulae are derived from first principles using Generalised Bond–slip Models.

One of the main benefits is that the Generalised Bond–slip Models can be transformed into various shapes. These can be achieved by altering shape constants (α and β) or by separating ascending and descending curves. Based on these principles, eight different bond–slip models can be deduced from these two Generalised Models, as shown in Fig. 7. The same deduction can be implemented to simplify the ultimate load resistance and effective length for all those eight deduced models.

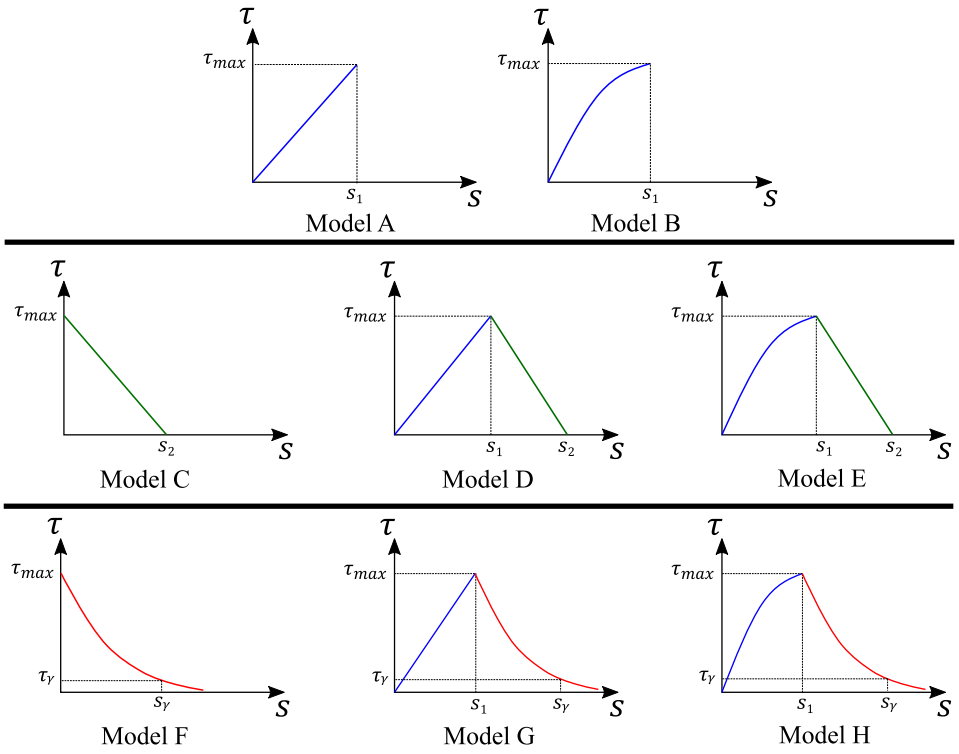

Fig. 7. The both Generalised Bond–slip Models are transformed into various possible shape of bond–slip models.

Table 1
Summary of the Generalised Bond–slip Models and derivations: effective bond length ($l_e = l_1 + l_2$) and maximum bond resistance ($F_{max} = F_{p,max} + F_{s,max}$); K value is the same for both Generalised Bond–slip Models, however this depends on the experimental set-up (double lap shear tests or single lap shear tests; ϵ_f is the strain with respected to distance along the bonded length; x and xx are the distance along the FRP for ascending and descending zones, respectively (See Fig. 3).

	Augusthus Nelson et al. (2020)	Present work
Generalised bond–slip models	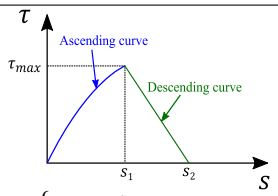 $\tau = \begin{cases} \tau_{max}\left(\frac{s}{s_1}\right)^{\alpha} & 0 \le s \le s_1 \\ \tau_{max}\left(\frac{s_2 - s}{s_2 - s_1}\right) & s_1 \le s \le s_2 \end{cases}$	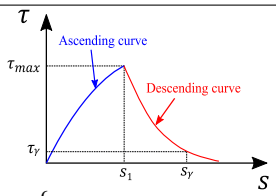 $\tau = \begin{cases} \tau_{max}\left(\frac{s}{s_1}\right)^{\alpha} & 0 \le s \le s_1 \\ \tau_{max} e^{-\beta(s - s_1)} & s_1 \le s \end{cases}$
Primary zone	$l_1 = \left(\frac{2(1+\alpha)}{K\rho_1(1-\alpha)^2}\right)^{\frac{1}{2}} s_1^{\frac{1-\alpha}{2}}$ $F_{p,max} = b_f \rho_1 \left(\frac{K\rho_1(1-\alpha)^2}{2(1+\alpha)}\right)^{\frac{\alpha}{1-\alpha}} l_1^{\frac{1+\alpha}{1-\alpha}}$ $\epsilon_f = \frac{\rho_1}{t_f E_f}\left(\frac{K\rho_1(1-\alpha)^2}{2(1+\alpha)}\right)^{\frac{\alpha}{1-\alpha}} x^{\frac{1+\alpha}{1-\alpha}}$	$l_1 = \left(\frac{2(1+\alpha)}{K\rho_1(1-\alpha)^2}\right)^{\frac{1}{2}} s_1^{\frac{1-\alpha}{2}}$ $F_{p,max} = b_f \rho_1 \left(\frac{K\rho_1(1-\alpha)^2}{2(1+\alpha)}\right)^{\frac{\alpha}{1-\alpha}} l_1^{\frac{1+\alpha}{1-\alpha}}$ $\epsilon_f = \frac{\rho_1}{t_f E_f}\left(\frac{K\rho_1(1-\alpha)^2}{2(1+\alpha)}\right)^{\frac{\alpha}{1-\alpha}} x^{\frac{1+\alpha}{1-\alpha}}$
Secondary zone	$l_2 = \frac{1}{\sqrt{K\rho_3}} \tan^{-1}\left(\frac{-B_2}{B_1}\right)$ $F_{s,max} = b_f \sqrt{\frac{\rho_3}{K}}\left(B_1 \cos\left(l_2\sqrt{K\rho_3}\right) - B_1 - B_2 \sin\left(l_2\sqrt{K\rho_3}\right)\right)$ $\epsilon_f = \frac{\left(F_{p,max} + b_f\sqrt{\frac{\rho_3}{K}}\left(B_1\cos\left(xx\sqrt{K\rho_3}\right) - B_1 - B_2\sin\left(xx\sqrt{K\rho_3}\right)\right)\right)}{t_f b_f E_f}$	$l_2 = \left(\frac{2}{\beta^2\gamma K\tau_{max}(1+\alpha)}\right)^{\frac{1}{2}}\left(\left(\gamma s_1 + (1+\alpha)(1-\gamma)\right)^{\frac{1}{2}} - (\gamma s_1)^{\frac{1}{2}}\right)$ $F_{s,max} = \frac{4b_f}{\beta^2 K\sqrt{P^2-4Q}} ln\left(\frac{l_2(P+\sqrt{P^2-4Q})+2Q}{l_2(P-\sqrt{P^2-4Q})+2Q}\right)^{\frac{1}{2}}$ $\epsilon_f = \frac{\left(F_{p,max} + \frac{4b_f}{\beta^2 K\sqrt{P^2-4Q}} ln\left(\frac{xx(P+\sqrt{P^2-4Q})+2Q}{xx(P-\sqrt{P^2-4Q})+2Q}\right)^{\frac{1}{2}}\right)}{t_f b_f E_f}$
Constants	$\rho_1 = \frac{\tau_{max}}{s_1^{\alpha}}$; $\rho_3 = \frac{\tau_{max}}{s_2 - s_1}$; $B_1 = \left(\frac{2\rho_1}{\rho_3(1+\alpha)}\right)^{\frac{1}{2}} s_1^{\frac{1+\alpha}{2}}$; $B_2 = s_1 - s_2$	$\rho_1 = \frac{\tau_{max}}{s_1^{\alpha}}$; $\gamma = \frac{\tau_\gamma}{\tau_{max}}$; $P = \frac{2}{\beta K\tau_{max}}\left(\frac{2K\rho_1}{(1+\alpha)}\right)^{\frac{1}{2}} s_1^{\frac{1+\alpha}{2}}$; $Q = \frac{2}{\beta^2 K\tau_{max}}$

4. Existing bond–slip models and parameters

4.1. Existing bond–slip models for epoxy bonded FRP to concrete

Most of the ascending and descending curves of the bond–slip models are represented by two separate mathematical functions, which are summarised in Appendix A.1. In few cases, a single mathematical equation was used to represent the ascending and descending curves, as illustrated in Appendix A.1. In the literature, the shapes of the ascending and descending curves varied from linear to exponential between bond–slip models. In addition to shape functions, the properties of the

Table 2
Summary of the shape and interfacial bond properties of existing bond–slip models and their dependability of the geometry and constitutive material properties.

Bond–slip models	Ascending curve			Descending curve		
	Power function			Linear	Exponential	
	τ_{max}	s_1	α	s_2	γ	β
Neubauer and Rostasy [29]	GC	G	1			
Monti et al. [30]	GC	GCA	1	G		
Brosens and Van Gemert [27]	GC	GCA	1	GC		
Ko et al. [31]	C	C	1	C		
Lu et al. [23] bi-linear model	GC	GC	1	GC		
Pan and Wu [16]	GC	GCA	1		–	GCA
Lu et al. [23] simplified model	GC	GC	0.5		–	GC
Dai and Ueda [38]	GCAF	GCAF	0.575		–	GAF

G = Geometry of the test sample; C = Mechanical properties of concrete;
A = Mechanical properties of epoxy glue; F = Mechanical properties of FRP

interfacial bond between FRP and concrete (τ_{max}, s_1 and s_2) are essential in developing the theoretical characteristics of bonded samples. Therefore, in Appendix, interfacial bond properties are summarised together with the shape functions of each bond–slip model.

A direct measurement of interfacial bond properties (τ_{max}, s_1 and s_2) is not possible from experimental investigations. Instead, researchers developed a strain profile of FRP along the bonded length and approximately converted the strain profile into a stress profile [35–37]. Using the stress and slip characteristics along the bonded length, an approximate bond–slip model was selected using statistical curve-fitting approaches [31]. For the selected bond–slip model, approximate interfacial bond properties with semi-empirical constants were then derived, as shown in Appendix. The number of experimental results used to validate those interfacial bond properties varied significantly and often increased chronologically.

4.2. Shape and interfacial bond parameters

It is understood that the shape and the interfacial bond parameters of a bond–slip model dictate theoretical predictions. To further improve understanding of the composition, the shape parameters (α, β and γ) and the interfacial bond parameters (τ_{max}, s_1 and s_2) of the bond–slip models with two separate mathematical functions for the ascending and descending curves are compared and critiqued in Table 2. As illustrated in Table 2, the shape of the ascending curve is defined as a constant in all those bond–slip models. Furthermore, as illustrated, the linear descending curve is also defined empirically. In contrast, exponentially decreasing curves are defined using the material properties of its constituent components (concrete, FRP, and epoxy glue) and the shape of the test samples. Moreover, the geometry of the test sample (except Ko et al.'s model) and material properties (concrete, FRP, and epoxy glue) of the system are used to define the interfacial bond–slip parameters of the models. It should be noted that the combination of material properties varies between the models, which are outlined in Appendix.

As identified, the parameters of the interfacial bond are defined in terms of the mechanical properties and geometries of concrete, FRP and adhesives. Obtaining mechanical properties and geometries of concrete and FPR is less controversial, and often standardised method of measurements were used. Hence, the adhesive's mechanical and physical properties (often thicknesses of the adhesive layers) are no commonly used in bond–slip models because of their complex nature, and obtaining these properties is cumbersome. For example, measurement of the thickness after application requires advanced optical distance measurement equipment because the thickness of the adhesive changes between samples as a result of the workmanship and the number of coatings applied. Dai et al. [39] measured the adhesive thickness in failed samples from bond–slip tests using a microscope. It was observed that the adhesive's thickness varies significantly between samples. Therefore, the thicknesses of the adhesive layer(s) were not reported in all of the experimental results found in the literature. Moreover, the mechanical behaviour of adhesive is nonlinear during the application of loading as the adhesive softens during the testing. Modelling such a complex nonlinear system is computationally overwhelming. Hence, the initial elastic and shear moduli of adhesives were used when and where the adhesive properties were considered [32,40]. Moreover, additional experimental tests of material are required to obtain elastic and shear moduli, unless the manufacturers provide them. To show the randomness of the properties of the adhesive, Table 3 summarises the adhesives used in the experimental investigations by Pan and Wu [16] and Dai et al. [39].

Table 3
Properties of adhesives.

Types of adhesives	Elastic modulus (GPa)	Poisson ratio	Shear modulus (GPa)
CN-100 [39]	0.39	0.45	0.13
SX-325 [39]	1.0	0.38	0.36
FR-E3P [39]	2.41	0.38	0.87
Adhesive [16]	3.5	0.4	1.25

4.3. Comparisons of shape and interfacial bond parameters

As illustrated in Appendix, the mathematical expressions for the interfacial bond parameters (τ_{max}, s_1 and s_2) and the shape parameters (α, β and γ) vary between the bond–slip models. Furthermore, the material properties (concrete, FRP, and adhesive) and combinations of these material properties are also different in mathematical expressions. As described, each available model at the time of development was calibrated using the part of the experimental results available in the literature. To illustrate the range of these parameters of interfacial bonds and understand the dependability of each component of the material, existing experimental results together with geometric and mechanical properties of the constitutive materials were collated from [6,8,41–50] (211 total test samples, 149 double-lap shear tests and 62 single shear-lap tests — only samples that meet the conditions in the derivations are selected for this validation).

The interfacial bond and shape parameters for each bond–slip model (using their model equations in column 4 Appendix) for all collated experimental samples are presented in Fig. 8. The bond–slip models that comply with the proposed Generalised Bond–slip Models 1 and 2 are used for this comparison. In addition, to make a direct comparison, the interfacial bond and shape parameters are grouped and presented according to the basic shape of the bond–slip models (Models A, D, G and H, as described in Fig. 7).

The plots along Fig. 8(b) are for the Neubauer and Rostasy model, where there is no direct comparison. The set of graphs in Fig. 8(b) are the bilinear bond–slip model and shows that τ_{max} is relatively consistent for all bond–slip models. Apparently, the deviation in τ_{max} is offset by changing s_1 and s_2. Fig. 8(c) is for the linearly ascending and exponentially descending bond–slip model, where there is no

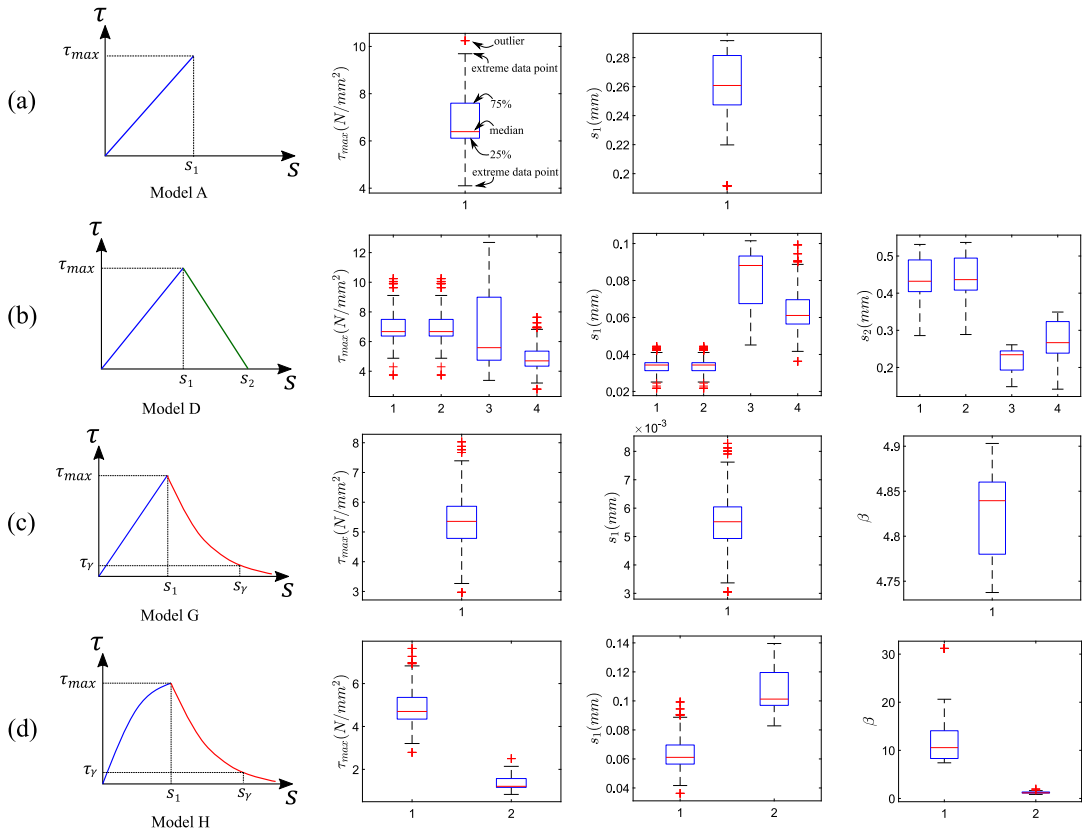

Fig. 8. Comparisons of shape and interfacial bond properties – outputs are grouped according to the shape of the models presented in Fig. 5 – (a) 1: Neubauer and Rostasy [29] (b) 1: Monti et al. [30], 2: Brosens and Van Gemert [27], 3: Ko et al. [31] and 4: Lu et al. [23] - bi-linear model (c) 1: Pan and Wu [16] (d) 1: Lu et al. [23] - simplified model, 2: Dai and Ueda [39]. On each box, the central mark (red horizontal line) indicates the median, and the bottom and top edges of the box indicate the 25th and 75th percentiles, respectively. The whiskers extend to the most extreme data points not considered outliers, and the outliers are plotted individually using the '+' symbol in red. (For interpretation of the references to colour in this figure legend, the reader is referred to the web version of this article.)

direct comparison. However, τ_{max} is very similar to what is observed in Fig. 8(b). In contrast, s_1 is significantly smaller. Fig. 8(d) is for nonlinearly ascending and exponentially descending, where Lu et al.'s simplified model and Dai and Ueda's model are compared. These are found to be significantly different.

4.4. Comparison of interfacial fracture energy

Even though the bond–slip models are different (as described in the section above), the method of estimating the interfacial fracture energy is the same. It is defined as the area under the bond–slip curves. As noted above, the interfacial bond and shape parameters are varied in all of the models reported here. It is debatable whether the various bond–slip parameters and shape variations matter or whether all of the models ultimately produce results with similar maximum bond resistance and effective bond length. Numerous works show that each bond–slip or bond-strength model gives different predictions. Fig. 9 compares the interfacial fracture energy of each model for all test samples. The comparison indicates that the interfacial fracture energies are very different, consistent with what is seen in Fig. 8. However, the interfacial fracture energies are well within the range reported by Biscaia et al. [24].

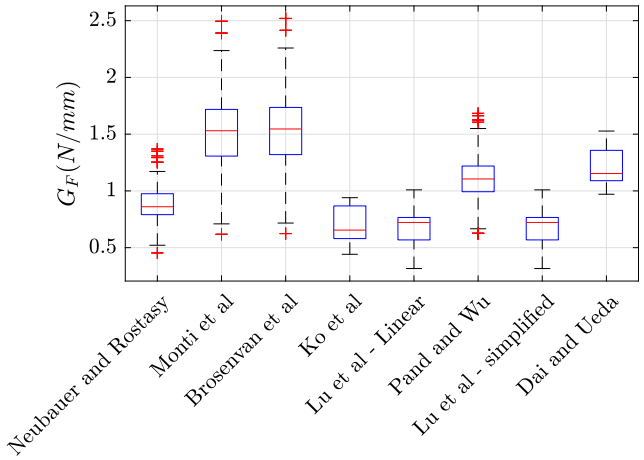

Fig. 9. Comparison of interfacial fracture energies all the existing bond–slip models considered in this study. On each box, the central mark (red horizontal line) indicates the median, and the bottom and top edges of the box indicate the 25th and 75th percentiles, respectively. The whiskers extend to the most extreme data points not considered outliers, and the outliers are plotted individually using the '+' symbol in red. (For interpretation of the references to colour in this figure legend, the reader is referred to the web version of this article.)

5. Validation of the theoretical derivations

The main aim of this paper is to show the use of derivations in predicting the responses of single- and double-lap bond tests. In addition, the secondary aim of this section are not to introduce a new set of interfacial bond and shape parameters; instead, the suitability of the bond–slip and shape parameters of existing models and the assumptions made for those bond–slip parameters are investigated using the derivations presented in this paper and Augusthus Nelson et al. [21].

5.1. Prediction of maximum load resistance

Any number of experimentally derived maximum load resistances can be used as a single data point for the maximum resistance when validating a proposed bond–slip model. Therefore, for the experimental results collated from the literature (see Section 4.3), the theoretical maximum load resistances for each bond–slip model with their interfacial bond and shape parameters were calculated using the derivations presented in this paper, and Augusthus Nelson et al. [21], summarised in Table 1.

Most of the existing experimental investigations of single and double lap shear tests report the properties of concrete and FRP with the geometry of the test samples. However, the properties of the adhesives are not reported in all of the experimental results. This is because measuring the thickness and elastic–plastic properties of epoxy is cumbersome. Therefore, an epoxy thickness of 0.9 mm, an elastic modulus of 2410 N/mm^2 and a Poisson's ratio of 0.4 are used in the prediction. In addition, if the FRP length of the sample is greater than the theoretical effective length, the maximum force resistance was calculated for the entire effective length. However, when the FRP lengths are shorter than the theoretical effective bond length, the primary and secondary zones were considered separately, and the maximum load resistance was calculated according to the length of the bonded FRP.

Furthermore, in theory, an infinite length is required to develop the entire bond–slip model for the exponentially descending curves. This is because the tail end of the exponential curve reaches zero bond stress at infinity. Therefore, defining the cutoff point beyond where the bonded stress can be negligible is necessary. In the derivations, the cutoff point (γ) for the effective length or effective bond resistance is defined in terms of fraction of maximum bond stress (τ_{max}) of the bond–slip model (see Eq. (29)). For this validation, $\gamma = 0.9$ is used.

The theoretical predictions of the maximum load resistance of each bond–slip model against the experimental load resistance are shown in Fig. 10. The comparison shows that the accuracy of the predictions improved from the single curve to the double curve bond–slip models. Additionally, the accuracy improved further when the descending curve changes from linear to exponential. However, interestingly, the bilinear models of Lu et al. provide a slightly better fit than the other models, as shown in Fig. 10.

5.2. Prediction of effective bond length

The effective length is defined as the extent of the FRP that must be bonded to a substrate to realise the complete bond–slip model, encompassing both its ascending and descending curves. As described before, a cutoff point is required for the bond–slip models with an exponentially descending curve. Therefore, as before, $\gamma = 0.9$ is used. The predictions of effective bond lengths using the theoretical derivations for each bond–slip model are presented in Fig. 11. It should be noted that quantifying the experimental effective bond length is not straightforward, as it cannot be measured explicitly from experiment. Image processing techniques have recently been used to quantify the effective bond length. However, such advanced techniques were not available in the early stages of the development of bond–slip models. Therefore, experimental measurements of effective bond lengths were not available in all of the experimental results reported in the literature. As a result, a direct comparison of the experimental and theoretical predictions cannot be reported here.

Researchers developed various empirical effective length models using the material and geometric properties of the bonded system, the interfacial fracture energy, or both. Again, theoretical predictions using the derivations reported here and the empirical predictions for each bond–slip model are not compared as this comparison is outside the scope of this article.

Appendix shows that α, which defines the shape of the ascending curve, varies between the bond–slip models. i.e., α is 0.5 and 1 in Lu et al.'s [23] and Pan and Wu's [16] models, respectively. Additionally, the derivation (Eq. (20)) demonstrates that when $\alpha = 1$, the denominator is zero, causing the effective length to reach infinity. Furthermore, the sensitivity studies by Augusthus Nelson et al. [21] show that α does not make a significant difference in the maximum load predictions, while the changes in effective length are observable. This study showed that $\alpha = 0.9$ gives reasonable accuracy for the bond–slip models that use $\alpha = 1$. Quantifiable continuous strain profiles along the FRP, which are difficult to measure during experimental investigations, are required to validate that α corresponds to the effective length. Therefore, $\alpha = 0.9$ is used for this validation when $\alpha = 1$, while the models of Lu et al. [23] and Dai and Udea [38] use 0.5 and 0.575, respectively.

The effective theoretical length is the bonded length required to develop the entire bond–slip curve. The infinite bond length is required

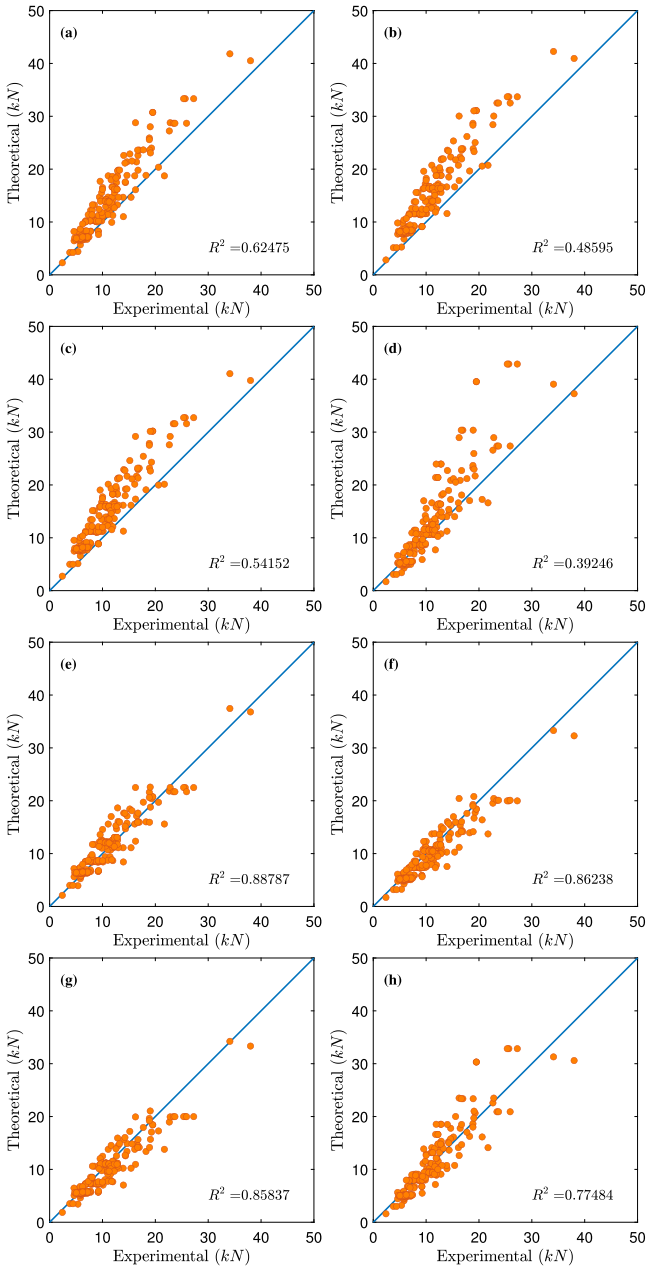

Fig. 10. Comparison between experimental results and theoretical prediction using parameters suggested by (a) Neubauer and Rostasy [29]; (b) Monti et al. [30]; (c) Brosens and Van Gemert [27]; (d) Ko et al. [31]; (e) Lu et al. [23] - bi-linear model; (f) Pan and Wu [16]; (g) Lu et al. [23] - simplified model; (h) Dai and Ueda [39].

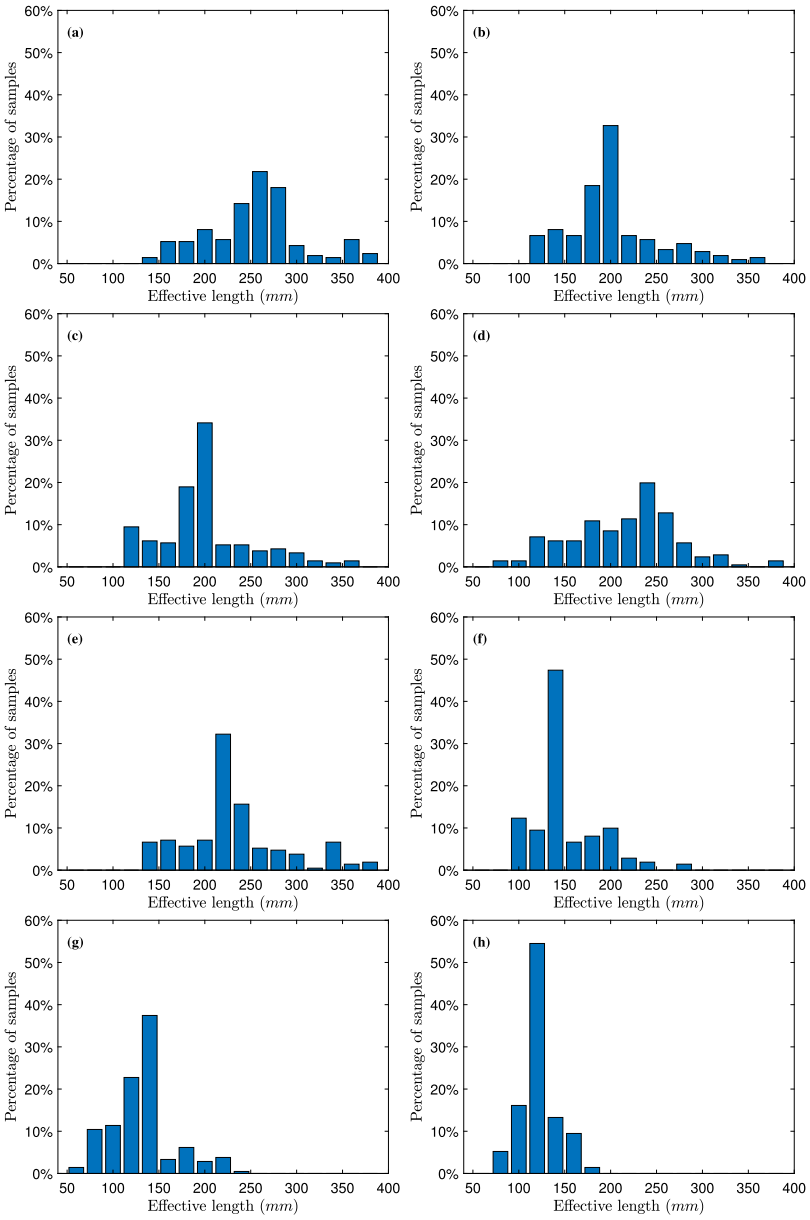

Fig. 11. Theoretical predictions of effective bond length using the parameters suggested by (a) Neubauer and Rostasy [29]; (b) Monti et al. [30]; (c) Brosens and Van Gemert [27]; (d) Ko et al. [31]; (e) Lu et al. [23] - bi-linear model; (f) Pan and Wu [16]; (g) Lu et al. [23] - simplified model; (h) Dai and Ueda [39].

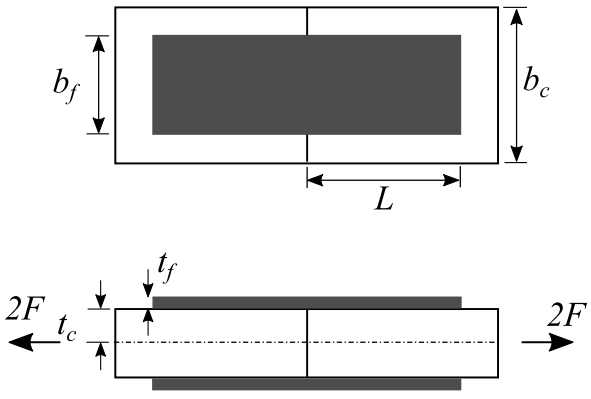

Fig. 12. Double lap shear test.

to develop an entire bond–slip curve in the exponentially descending bond–slip models. Therefore, various cut-off points concerning maximum load resistance and the effective length were studied [51,52]. Cornetti and Carpinteri's [53] studies showed that the cutoff point of the exponentially descending curve does not significantly influence the maximum load resistance or the load–deflection response. However, the effective length varied considerably with varying cutoff points. This can be attributed to the changes in the cutoff point which do not significantly alter the interfacial fracture energy. Therefore, the cut-off point for exponential descending curves was calculated to form the known interfacial fracture energy once the characteristics of the ascending curve were established [16]. The load–deformation comparison between the experimental output and the theoretical prediction using an exponential descending curve with 10% cut-off point showed acceptable agreement. Hence, 0.9 is used in this study.

As expected, effective length predictions are inconsistent, as shown in Fig. 11. The linearly ascending bond–slip curve leads to an infinite effective bond length. However, Lu et al.'s [23] and Dai and Udea's [38]

Table 4
Mechanical properties of concrete, FRP and epoxy glue.

Concrete	Cube strength, f_{cu}	41.6 N/mm^2
	Tensile strength, f_t	4.2 N/mm^2
	Young's elastic modulus, E_c	29,670 N/mm^2
FRP	Tensile strength, f_f	4,000 N/mm^2
	Young's elastic modulus, E_f	240 × 10^{3}N/mm^2
Epoxy glue	Poisson ratio, υ_a	0.4
	Young's elastic modulus, E_a	2400 N/mm^2
	Thickness, t_a	0.9 mm

models use non-linear ascending curves and give finite effective bond lengths. The same issue exists between the linearly and exponentially descending curves, as the linearly descending curve gives finite effective bond length while the exponentially descending curve gives infinite effective bond length. The calibration of these models is not feasible, as the direct measurement of effective length from experimental investigations is not feasible. However, as shown in Fig. 11, the prediction of effective bond length is possible for any combination of ascending and descending curves using the analytical derivations presented here.

5.3. Load slip curve

To demonstrate the derivation presented in this article and Augusthus-Nelson et al. [21], double lap shear experimental samples tested by Al-Allaf et al. are used in this section, as shown in Fig. 12. The bonded length of the FRP (L) is 100 mm, and the thickness (t_f) and width (b_f) of the FRP are 0.117 mm and 100 mm, respectively. The width and thickness of the concrete (half of the total width) are 200 mm and 45 mm, respectively. Table 4 lists the characteristics of concrete, FRP, and epoxy. It should be noted that the properties of epoxy are approximate and depend on the manufacturer's recommendations rather than being measured. A detailed test plan can be found elsewhere [8,50,54].

Fig. 13(a) and (b) compare the shapes (including interfacial bond parameters) and interfacial fracture energies, respectively, for each of the eight bond–slip models for the test sample of Al-Allaf et al. As shown in Fig. 13(a), the bond–slip models differ widely. The model of Neubauer and Rostasy (specified by a single linear curve) differs significantly from other bond–slip models, when compared. Furthermore, the models developed by Monti et al. and Brosens and Van Gemert are nearly identical. Both the bilinear (linearly ascending and descending) and simplified (nonlinearly ascending and exponentially descending) models of Lu et al. are comparable to Ko et al. which is solely dependent on the compressive strength of concrete. In the literature, the interfacial fracture energy is used when developing the comparison. Therefore, the interfacial fracture energies of each bond–slip model are compared in Fig. 13(b). As observed, the fracture energies are widely different too. The question arises of which bond–slip model is best for predicting the behaviour.

The theoretical load-slip predictions using these bond–slip models for Al-Allaf et al. are plotted against the experimental results in Fig. 14. Neubauer and Rosstasy's prediction is significantly different from experimental results. This behaviour is the same as that for Monti et al. and the Brosens and Van Gemert models. Initial stiffness of Ko et al.'s and Lu et al.'s bilinear models are marginally different from experimental results. However, this difference becomes greater as the load increased. The prediction of Pan and Wu is very similar to the experimental results. Lu et al.'s simplified and Dai and Udea's models are similar at the start of the load–deformation curve. However, the theoretical load–deformation curves are terminated because the bonded length of the FRP was only 100 mm (the theoretical effective bond length is greater than 100 mm for both bond–slip models) for the test sample of Al-Allaf et al.

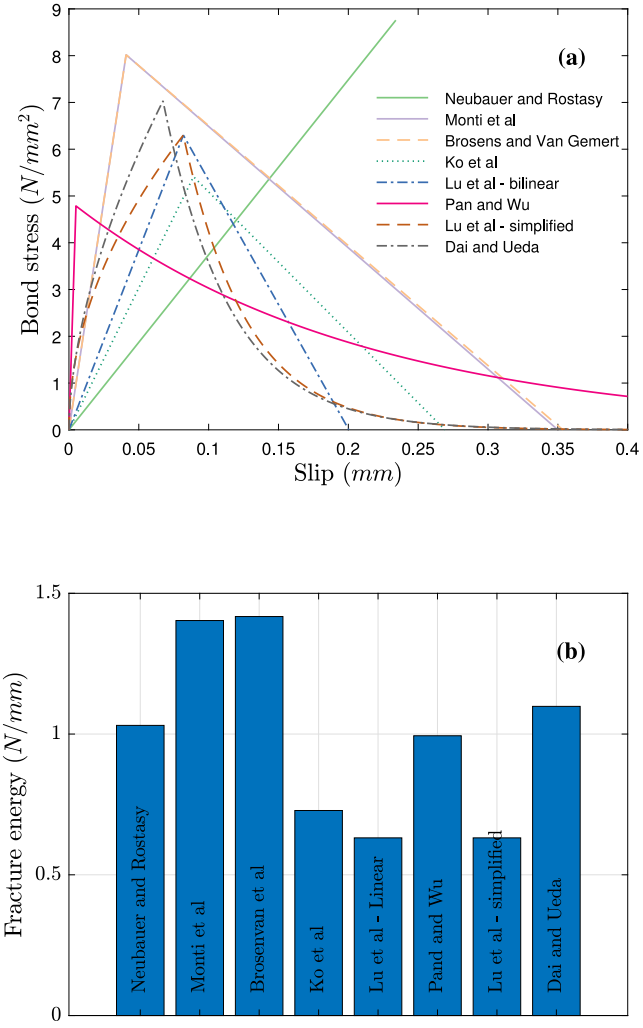

Fig. 13. (a) Bond–slip curves and (b) interfacial fracture energies for Al-Allaf et al.'s test samples.

5.4. Prediction of strain distribution

As shown, the mathematical derivations presented in Section 2 in this paper and Augusthus Nelson et al. [21] allow the construction of a complete strain profile along the bonded length of FRP, demonstrated in Fig. 15. All eight different bond–slip models, as before, have been used with the experimental setup of Al-Allaf et al. (see Fig. 12 and Table 4).

Fig. 15(a) shows the strain profile along the FRP for the fully developed ascending curve of Neubauer and Rostasy's bond–slip model, which is defined using a single linearly ascending curve (the inset shows the bond–slip model for the experimental sample of Al-Allaf et al.). In Fig. 15(b), the solid line on the left illustrates the strain profile for the fully developed ascending curve of Monti et al.'s bond–slip model, which corresponds to the stage described in Fig. 5(c). As mentioned, the ascending curve shifts towards the unloaded end when the load increases, thus allowing the descending curves to develop. The curve in the middle (with solid and hidden lines) represents the strain profile for the fully developed ascending curves (solid line) and partially developed descending curves (hidden line), which corresponds to the stage described in Fig. 5(d). With increasing applied load, both the ascending and descending curves are fully developed, as shown by the curve on the right, which corresponds to the stage described in Fig. 5(e). According to bond–slip models, the fully developed strain

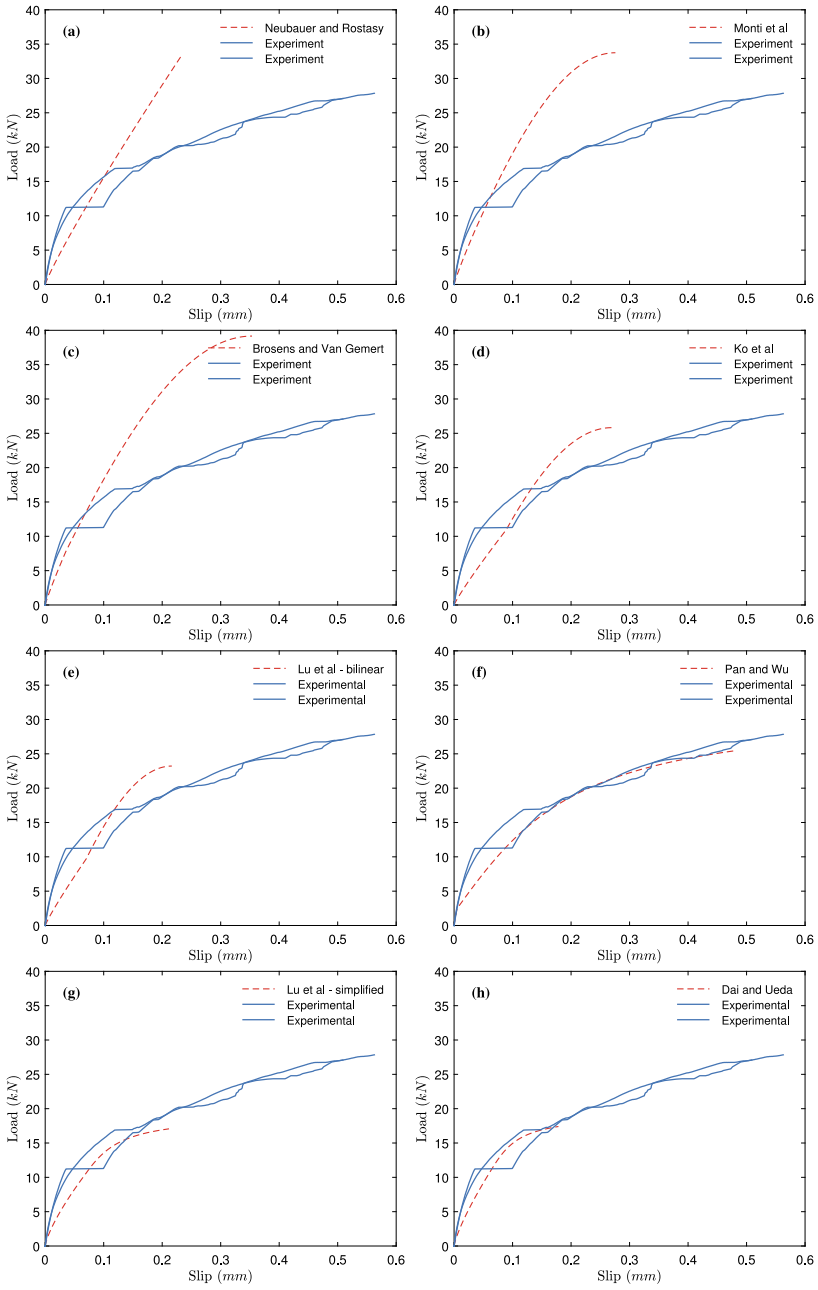

Fig. 14. Load-slip comparisons between experimental results and theoretical prediction using parameters suggested by (a) Neubauer and Rostasy [29]; (b) Monti et al. [30]; (c) Brosens and Van Gemert [27]; (d) Ko et al. [31]; (e) Lu et al. [23] - bi-linear model; (f) Pan and Wu [16]; (g) Lu et al. [23] - simplified model; (h) Dai and Ueda [39].

profile (curve on the right with solid and hidden lines) shifts towards the unloaded end with increasing load. The strain profiles are the same for all the bond–slip models (the corresponding bond–slip models are provided in the inset), as shown in the subfigures of Fig. 15. The strain profiles on the right (fully developed ascending and descending curves of each bond–slip model) can also be used to establish the effective length of the bond.

6. Conclusion

Various bond–slip models have been proposed in the literature for FRP-bonded concrete. In each model, different mathematical formulations for shape and interfacial bond characteristics were developed. Out of all the bond–slip models, a small number are defined by a single mathematical expression. The rest are defined using two mathematical expressions (each expression for ascending and descending part of the bond–slip model). The most prevalent ascending curve of the bond–slip model is linear or comprised of power functions, while the descending curve is linear or exponential functions.

For accurate prediction, the bond–slip model must be validated before being used in a structural retrofitting study. However, the bond–slip model is an implicit characteristic. Therefore, three approaches were considered to develop experimental outputs to validate the bond–slip model: empirical mathematical expressions (empirical constants were developed or calibrated from the curve fitting with the experimental results), numerical or finite element analysis using computer software packages, and closed-form analytical solutions.

Firstly, most mathematical expressions with empirical constants were developed to predict the maximum load resistance and effective bond length for a specific bond–slip model. However, only a few empirical expressions that would allow for predicting the load–deformation (or slip) response and strain distribution along the bonded FRP length

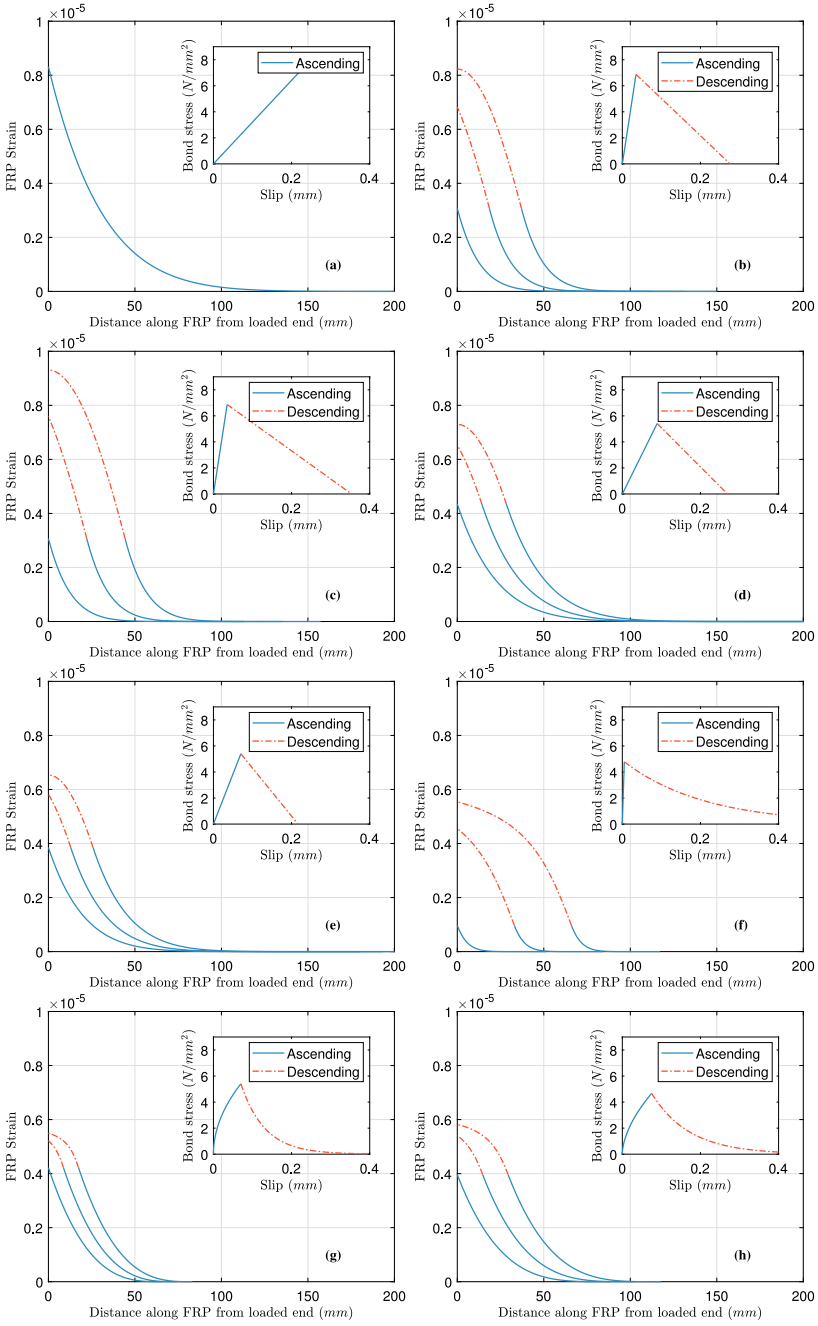

Fig. 15. Theoretical predictions of strain in FRP along the bonded FRP length using the bond–slip parameters suggested by (a) Neubauer and Rostasy [29]; (b) Monti et al. [30]; (c) Brosens and Van Gemert [27]; (d) Ko et al. [31]; (e) Lu et al. [23] - bi-linear model; (f) Pan and Wu [16]; (g) Lu et al. [23] - simplified model; (h) Dai and Ueda [39]. The inset plots in each subplot shows the bond–slip model. The blue solid line represents the ascending portion of the bond–slip model, while the red hidden line represents the descending portion of the bond–slip model.

were proposed. The main challenge of this approach is that a specific mathematical expression only applies to a specific bond–slip model. Furthermore, the empirical constant will vary depending on the number of experimental results used to calibrate. Therefore, the suitability of the approach is limited even though it provides a prediction.

The second approach was to validate the bond–slip models using a numerical approach (i.e. finite element analysis). This approach provides a powerful in-depth understanding of the test sample. However, the modelling of each sample should be performed one by one. Therefore, validating the bond–slip with numerous experimental results may be challenging.

Closed-form analytical solutions developed from first principles avoid the validation of each test sample one by one and use empirical constants to predict experimental outputs. It should also be noted that the closed-form analytical solutions are limited to bond failure between concrete and FRP, while FRP and concrete remain elastic. Therefore, concrete fracture failure or FRP rupture should be modelled as a material failure. This is beyond the scope of this paper. The earliest closed-form analytical solutions are specific to the shape of the bond–slip curve, and therefore, it does not apply to other shapes. Also, the analytical solutions are only for specific experimental outputs.

The complete and comprehensive closed-form analytical solutions presented in this paper and those of Augusthus Nelson et al. [21] are for the generalised bond–slip models. The generalised bond–slip models can be transformed into several bond–slip models, defined by the combination of linear or power ascending curves and linear or

exponential descending curves. In addition, the generalised bond–slip model and thus derivations can be deduced to single curved bond–slip models. Furthermore, unlike any bond–slip models previously proposed in the literature, all of the typical outputs from experimental tests (maximum load resistance, effective length prediction, complete construction of load–deformation (slip) curves, and strain profile along bonded FRP length) can be numerically driven using the derivations presented in this paper and Augusthus Nelson et al. [21]. As discerned from our observations, the prediction of load resistance capacity is intrinsically governed by the interfacial fracture energy. Consequently, in this context, it is pertinent to note that Lu et al.'s bi-linear model, meticulously calibrated using an extensive dataset, as well as all the exponentially descending bond–slip models, including the Pan and Wu model, Lu et al.'s simplified model, and Dai and Udea model, exhibited superior predictive performance. Notably, the exponentially descending bond–slip models, in particular, exhibited a closer alignment with the experimental load-slip response when compared with their linearly descending counterparts. Furthermore, congruent trends with the experimental outcomes were observed when examining the predictions of effective length and strain along the FRP. Therefore, to gain a deeper understanding of these bond–slip models, considering their characteristics and shapes, it becomes imperative to conduct a sensitivity analysis of the pertinent bond parameters.

CRediT authorship contribution statement

Levingshan Augusthus Nelson: Conceptualization, Methodology, Formal analysis, Software, Data Curation, Writing – original draft, Visualization. **Laurence Weekes:** Formal analysis, Resources, Writing – review & editing, Supervision. **Gabriele Milani:** Formal analysis, Software, Writing – review & editing. **Mustafa Al-Allaf:** Investigation, Resources.

Declaration of competing interest

Authors have no conflict of interests for this paper.

Data availability

Data will be made available on request.

Appendix. Existing bond–slip models and their interfacial bond properties

See Table A.1.

Table A.1
A summary of the bond-slip models that have been studied and presented in the literature to demonstrate how FRP adheres to concrete.

Model Fig. 7	Bond–slip model	Ascending (primary)	Descending (secondary)	Bond–slip parameters
A	Neubauer and Rostasy [29]	$\tau_{max}\frac{s}{s_1}$	0	$\tau_{max}=1.8\beta_w f_t$ $\alpha=1$ $s_1=0.202\beta_w$ $s_2=s_1$ $\beta_w=\sqrt{\frac{1.125(2-b_f/b_c)}{1+b_f/400}}$
D	Monti et al. [30]	$\tau_{max}\frac{s}{s_1}$	$\tau_{max}\frac{s_2-s}{s_2-s_1}$	$\tau_{max}=1.8\beta_w f_t$ $\alpha=1$ $s_1=2.5\tau_{max}\left(\frac{t_a}{E_a}+\frac{50}{E_c}\right)$ $s_2=0.33\beta_w$ $\beta_w=\sqrt{\frac{1.5(2-b_f/b_c)}{1+b_f/100}}$
D	Brosens and Van Gemert [27,28]	$\tau_{max}\frac{s}{s_1}$	$\tau_{max}\frac{s_2-s}{s_2-s_1}$	$\tau_{max}=1.8\beta_w f_t$ $\alpha=1$ $s_1=2.5\tau_{max}\left(\frac{t_a}{E_a}+\frac{50}{E_c}\right)$ $s_2=\frac{2G_f}{\tau_{max}}$ $\beta_w=\sqrt{\frac{1.5(2-b_f/b_c)}{1+b_f/100}}$ $G_f=0.3\beta_w^2 f_t$
D	Ko et al. [31]	$\tau_{max}\frac{s}{s_1}$	$\tau_{max}\frac{s_2-s}{s_2-s_1}$	$\tau_{max}=0.165 f_c$ $\alpha=1$ $s_1=0.122-0.001 f_c$ $s_2=0.302-0.002 f_c$
D	Lu et al. [23] bi-linear model	$\tau_{max}\frac{s}{s_1}$	$\tau_{max}\frac{s_2-s}{s_2-s_1}$	$\tau_{max}=1.5\beta_w f_t$ $\alpha=1$ $s_1=0.0195\beta_w f_t$ $s_2=\frac{0.616\beta_w^2\sqrt{f_t}}{\tau_{max}}$ $\beta_w=\sqrt{\frac{2-b_f/b_c}{1+b_f/b_c}}$
G	Pan and Wu [16]	$\tau_{max}\frac{s}{s_1}$	$\tau_{max}e^{-\beta(s-s1)}$	$\frac{\tau_{max}}{E_d}=1.31k_w^2\left(\frac{f_c}{E_d}\right)^{0.19}$ $\alpha=1$ $s_1=\frac{\tau_{max}}{k}$ $\beta=\frac{\tau_{max}}{G_f}$ $\frac{G_f}{E_d d}=0.247k_w^2\left(\frac{f_c}{E_d}\right)^{0.216}$ $k=\frac{G_a}{t_a}$ $k_w=\lambda'+(1-\lambda')\frac{b_f}{b_c}$ $\lambda'=1+0.222\left(\frac{f_c}{E_d}\right)^{0.304}$ $E_d=1MPa; d=1$ m

(continued on next page)

Table A.1 (*continued*).

H	Lu et al. [23] simplified model	$\tau_{max}\left(\frac{s}{s_1}\right)^{\frac{1}{2}}$	$\tau_{max}e^{-\beta(s-s_1)}$	$\tau_{max}=1.5\beta_w f_t$ $\alpha=\frac{1}{2}$ $s_1=0.0195\beta_w f_t$ $\beta=\frac{1}{\frac{G_f}{\tau_{max}}-\frac{2s_1}{3}}$ $\beta_w=\sqrt{\frac{2-b_f/b_c}{1+b_f/b_c}}$ $G_f=0.308\beta_w^2\sqrt{f_t}$
H	Dai and Ueda [38]	$\tau_{max}\left(\frac{s}{s_1}\right)^{0.575}$	$\tau_{max}e^{-\beta(s-s_1)}$	$\tau_{max}=\frac{1}{2\beta}\left(-1.575\psi K_a+\sqrt{2.481\psi^2K_a^2+6.3\psi\beta^2K_aG_f}\right)$ $\alpha=0.575$ $s_1=\frac{\tau_{max}}{\psi K_a}$ $\beta=0.0035K_a\left(\frac{E_f t_f}{1000}\right)^{0.34}$ $\psi=0.028\left(\frac{E_f t_f}{1000}\right)^{0.254}$ $G_f=7.554K_a^{-0.449}f_c^{0.343}$ $K_a=\frac{G_a}{t_a}$
	Lu et al. [23] precise model	$\tau_{max}\sqrt{\frac{s}{s_1A}+B^2}+B$	$\tau_{max}e^{-\beta(s-s_1)}$	$\tau_{max}=1.5\beta_w f_t$ $s_1=0.0195\beta_w f_t+\frac{\tau_{max}(G_a t_c+G_c t_a)}{G_a G_c}$ $\beta=\frac{\tau_{max}}{G_f-G_f^a}$ $\beta_w=\sqrt{\frac{2-b_f/b_c}{1+b_f/b_c}}$ $G_f=0.308\beta_w^2\sqrt{f_t}$ $G_f^a=\tau_{max}s_1\left[\frac{2A}{3}\left(\frac{1+B^2A}{A}\right)^{\frac{3}{2}}-B-\frac{2}{3}B^3A\right]$ $A=\frac{0.0195\beta_w f_t}{s_1}$ $B=\frac{1}{0.039\beta_w f_t}\frac{\tau_{max}(G_a t_c+G_c t_a)}{G_a G_c}$
	Baky et al. [33]	$E_o s+(\tau_{max}-E_o s_1)\left(\frac{s}{s_1}\right)^3$	$\tau_{max}e^{-\beta(s-s_1)}$	$\tau_{max}=\frac{2f_t}{-\psi+\sqrt{\psi^2+4}}$ $\gamma=0.1$ $s_1=\tau_{max}\left(0.35\frac{t_f}{G_{ff}}+8.5\frac{t_a}{G_a}+3\frac{t_c^-}{G_c}\right)$ $\beta=\frac{0.9\tau_{max}}{G_f^p}$ $G_f^p=\tau_{max^2}\left[\frac{150}{G_c}-0.405\left(\frac{t_f}{G_{ff}}+\frac{t_a}{4.25G_a}\right)\right]$ $\lambda^2=\frac{G_a}{E_f t_f t_a}\left(1+\frac{E_f A_f}{E_c A_c}\right)$ $\psi=\frac{A_f}{\lambda A_c t_f}$ $\frac{1}{E_o}=\frac{t_f}{G_{ff}}+\frac{t_a}{G_a}+\frac{t_c^-}{G_c}$
	Nakaba et al. [55]	$\tau_{max}\frac{s}{s_1}\left(3/\left(2+(s/s_1)^3\right)\right)^+$		$\tau_{max}=3.5f_c^{0.19}$ $s_1=0.065$
	Savioa et al. [56]	$\tau_{max}\frac{s}{s_1}\left(2.86/\left(1.86+(s/s_1)^{2.86}\right)\right)^+$		$\tau_{max}=3.5f_c^{0.19}$ $s_1=0.051$
	Dai et al. [39]	$2BG_f\left(e^{-Bs}-e^{-2Bs}\right)^+$		$\tau_{max}=0.5BG_f$ $s_1=0.693B$ $B=6.846(E_f t_f)^{0.108}\left(\frac{G_a}{t_a}\right)^{0.833}$ $G_f=0.446(E_f t_f)^{0.023}\left(\frac{G_a}{t_a}\right)^{-0.352}f_c^{0.236}$
FRP Reinforcement: b_f = width; t_f = thickness; E_f = elastic; G_{ff} = shear modulus.				
Concrete: b_c = width; t_c = thickness; E_c = elastic Young's modulus; f_t = tensile strength; f_c = cylinder strength; G_c = shear modulus; t_c^- = thin inter-facial layer (Baky et al's model consider less than t_c).				
Epoxy glue: t_a = thickness; E_a = elastic Young's modulus; G_a = shear modulus.				
G_f = Fracture toughness (each model provides different formulae) + single curve				

References

[1] De Lorenzis L, Miller B, Nanni A. Bond of FRP laminates to concrete. ACI Mater J 2001;98(3):256–64.

[2] Pilakoutas K, Guadagnini M, Neocleous K, Matthys S. Design guidelines for FRP reinforced concrete structures. Proc Inst Civ Eng - Struct Build 2011;164(4):255–63. http://dx.doi.org/10.1680/stbu.2011.164.4.255, URL https://www.icevirtuallibrary.com/doi/10.1680/stbu.2011.164.4.255.

[3] Triantafillou TC, Plevris N. Strengthening of RC beams with epoxy-bonded fibre-composite materials. Mater Struct 1992 25:4 1992;25(4):201–11. http://dx.doi.org/10.1007/BF02473064, URL https://link.springer.com/article/10.1007/BF02473064.

[4] Tighiouart B, Benmokrane B, Gao D. Investigation of bond in concrete member with fibre reinforced polymer (FRP) bars. Constr Build Mater 1998;12(8):453–62. http://dx.doi.org/10.1016/S0950-0618(98)00027-0.

[5] Hoult NA, Lees JM. Efficient CFRP strap configurations for the shear strengthening of reinforced concrete T-beams. J Compos Constr 2009;13(1):45–52. http://dx.doi.org/10.1061/(ASCE)1090-0268(2009)13:1(45).

[6] Yao J, Teng JG, Chen JF. Experimental study on FRP-to-concrete bonded joints. Composites B 2005;36(2):99–113. http://dx.doi.org/10.1016/j.compositesb.2004.06.001.

[7] Bilotta A, Ludovico MD, Nigro E. FRP-to-concrete interface debonding: Experimental calibration of a capacity model. Composites B 2011;42(6):1539–53. http://dx.doi.org/10.1016/j.compositesb.2011.04.016.

[8] Al-Allaf MH, Weekes L, Augusthus-Nelson L, Leach P. An experimental investigation into the bond-slip behaviour between CFRP composite and lightweight concrete. Constr Build Mater 2016;113:15–27. http://dx.doi.org/10.1016/j.conbuildmat.2016.03.032.

[9] Serbescu A, Guadagnini M, Pilakoutas K. Standardised double-shear test for determining bond of FRP to concrete and corresponding model development. Composites B 2013;55:277–97. http://dx.doi.org/10.1016/j.compositesb.2013.06.019.

[10] Chen JF, Teng JG. Anchorage strength models for FRP and steel plates bonded to concrete. J Struct Eng 2001;127(7):784–91.

[11] Khalifa A, Gold WJ, Nanni A, MI AA. Contribution of externally bonded FRP to shear capacity of RC flexural members. J Compos Construct 1998;2(4):195–202.

[12] Yuan H, Teng JG, Seracino R, Wu ZS, Yao J. Full-range behavior of FRP-to-concrete bonded joints. Eng Struct 2004;26(5):553–65.

[13] Wang J. Cohesive zone model of FRP-concrete interface debonding under mixed-mode loading. Int J Solids Struct 2007;44(20):6551–68. http://dx.doi.org/10.1016/j.ijsolstr.2007.02.042.

[14] Fawzia S, Zhao X-L, Al-Mahaidi R. Bond–slip models for double strap joints strengthened by CFRP. Compos Struct 2010;92(9):2137–45. http://dx.doi.org/10.1016/j.compstruct.2009.09.042, URL https://linkinghub.elsevier.com/retrieve/pii/S0263822309003821.

[15] Ali-Ahmad M, Subramaniam K, Ghosn M. Experimental investigation and fracture analysis of debonding between concrete and FRP sheets. J Eng Mech 2006;132(9):914–23. http://dx.doi.org/10.1061/(ASCE)0733-9399(2006)132:9(914), URL https://ascelibrary.org/doi/10.1061/%28ASCE%290733-9399%282006%29132%3A9%28914%29.

[16] Pan J, Wu YF. Analytical modeling of bond behavior between FRP plate and concrete. Composites B 2014;61:17–25. http://dx.doi.org/10.1016/j.compositesb.2014.01.026.

[17] Al-Rousan R, Issa M. Fatigue performance of reinforced concrete beams strengthened with CFRP sheets. Constr Build Mater 2011;25(8):3520–9.

[18] Ghiassi B, Xavier J, Oliveira DV, Lourenço PB. Application of digital image correlation in investigating the bond between FRP and masonry. Compos Struct 2013;106:340–9. http://dx.doi.org/10.1016/j.compstruct.2013.06.024, URL https://linkinghub.elsevier.com/retrieve/pii/S0263822313003176.

[19] Zhu H, Wu G, Shi J, Liu C, He X. Digital image correlation measurement of the bond-slip relationship between fiber-reinforced polymer sheets and concrete substrate. J Reinf Plast Compos 2014;33(17):1590–603. http://dx.doi.org/10.1177/0731684414541017/ASSET/IMAGES/LARGE/10.1177{_}0731684414541017-FIG2.JPEG, URL https://journals.sagepub.com/doi/full/10.1177/0731684414541017?casa_token=8RjxoFOLEtMAAAAA%3Ar1x9FDpZ45ww_kPRa7ZIkv-nzfeLYeuv8cVpfPV0E7FAuZvAkMwu8pokPELy0j1tSkFBsp3Y29jO.

[20] Wu YF, Xu XS, Sun JB, Jiang C. Analytical solution for the bond strength of externally bonded reinforcement. Compos Struct 2012;94(11):3232–9. http://dx.doi.org/10.1016/j.compstruct.2012.04.026.

[21] Augusthus L, Al-allaf M, Weekes L. Analytical modelling of bond-slip failure between epoxy bonded FRP and concrete substrate. Compos Struct 2020;251(June):112596. http://dx.doi.org/10.1016/j.compstruct.2020.112596.

[22] Mazzotti C, Savoia M, Ferracuti B. An experimental study on delamination of FRP plates bonded to concrete. Constr Build Mater 2008;22(7):1409–21. http://dx.doi.org/10.1016/j.conbuildmat.2007.04.009.

[23] Lu XZ, Teng JG, Ye LP, Jiang JJ. Bond-slip models for FRP sheets/plates bonded to concrete. Eng Struct 2005;27(6):920–37. http://dx.doi.org/10.1016/j.engstruct.2005.01.014.

[24] Biscaia HC, Chastre C, Silva MA. Linear and nonlinear analysis of bond-slip models for interfaces between FRP composites and concrete. Composites B 2013;45(1):1554–68. http://dx.doi.org/10.1016/j.compositesb.2012.08.011.

[25] Dehghani E, Daneshjoo F, Aghakouchak AA, Khaji N. A new bond-slip model for adhesive in CFRP–steel composite systems. Eng Struct 2012;34:447–54.

[26] Liu K, Wu Y-F. Analytical identification of bond–slip relationship of EB-FRP joints. Composites B 2012;43(4):1955–63.

[27] Brosens K, Van Gemert D. Plate end shear design for external CFRP laminates, vol. 3. In: Fracture mechanics of concrete structures. AEDIFICATIO Publishers; 1998, p. 1793–804.

[28] Brosens K, Van Gemert D. Anchorage design for externally bonded carbon fiber reinforced polymer laminates. Special Publ 1999;188:635–46.

[29] Neubauer U, Rostasy FS. Bond failure of concrete fiber reinforced polymer plates at inclined cracks—experiments and fracture mechanics model. Special Publ 1999;188:369–82.

[30] Monti G, Renzelli M, Luciani P. FRP adhesion in uncracked and cracked concrete zones. In: Fibre-reinforced polymer reinforcement for concrete structures: (in 2 Volumes). World Scientific; 2003, p. 183–92.

[31] Ko H, Matthys S, Palmieri A, Sato Y. Development of a simplified bond stress-slip model for bonded FRP-concrete interfaces. Constr Build Mater 2014;68:142–57. http://dx.doi.org/10.1016/j.conbuildmat.2014.06.037.

[32] Dai JG, Sato Y, Ueda T. Improving the load transfer and effective bond length for frp composites bonded to concrete. Proc Jpn Concr Inst 2002;24(March 2015):1423–8.

[33] Baky HA, Ebead UA, Neale KW. Nonlinear micromechanics-based bond–slip model for FRP/concrete interfaces. Eng Struct 2012;39:11–23.

[34] Wu YF, Jiang C. Quantification of bond-slip relationship for externally bonded FRP-to-concrete joints. J Compos Construct 2013;17(5):673–86. http://dx.doi.org/10.1061/(ASCE)CC.1943-5614.0000375.

[35] Pellegrino C, Tinazzi D, Modena C. Experimental study on bond behavior between concrete and FRP reinforcement. J Compos Construct 2008;12(2):180–9.

[36] Dai J-G, Gao WY, Teng JG. Bond-slip model for FRP laminates externally bonded to concrete at elevated temperature. J Compos Constr 2013;17(2):217–28.

[37] Lin X, Zhang YX. Bond–slip behaviour of FRP-reinforced concrete beams. Constr Build Mater 2013;44:110–7.

[38] Dai JG, Ueda T. Local bond stress slip relations for FRP sheets-concrete interfaces. In: Fibre-reinforced polymer reinforcement for concrete structures: (in 2 Volumes). World Scientific; 2003, p. 143–52.

[39] Dai J, Ueda T, Sato Y. Development of the nonlinear bond stress–slip model of fiber reinforced plastics sheet–concrete interfaces with a simple method. J Compos Construct 2005;9(1):52–62. http://dx.doi.org/10.1061/(asce)1090-0268(2005)9:1(52).

[40] Lee YJ, Boothby TE, Bakis CE, Nanni A. Slip modulus of FRP sheets bonded to concrete. J Compos Construct 1999;3(4):161–7.

[41] Bizindavyi L, Neale KW. Transfer lengths and bond strengths for composites bonded to concrete. J Compos Construct 1999;3(4):153–60.

[42] Tan Z. Experimental research for RC beam strengthened with GFRP (Graduation thesis), Beijing, China (in Chinese): Tsinghua Univ.; 2002.

[43] Zhao HD, Zhang Y, Zhao M. Research on the bond performance between CFRP plate and concrete. In: Proc., 1st conf. on FRP concrete structures of china. 2000, p. 247–53.

[44] Takeo K, Matsushita H, Makizumi T, Nagashima G. Bond characteristics of CFRP sheets in the CFRP bonding technique. Proc Jpn Concr Inst 1997;19(2):1599–604.

[45] Ren HT. Study on basic theories and long time behavior of concrete structures strengthened by fiber reinforced polymers. Dalian University of Technology; 2003.

[46] Ueda T, Sato Y, Asano Y. Experimental study on bond strength of continuous carbon fiber sheet. Special Publ 1999;188:407–16.

[47] Wu Z, Yuan H, Yoshizawa H, Kanakubo T. Experimental/analytical study on interfacial fracture energy and fracture propagation along frp-concrete i nterface. Special Publ 2001;201:133–52.

[48] Toutanji H, Saxena P, Zhao L, Ooi T. Prediction of interfacial bond failure of FRP–concrete surface. J Compos Construct 2007;11(4):427–36.

[49] Chajes MJ, Finch WW, Thomson TA. Bond and force transfer of composite-material plates bonded to concrete. Struct J 1996;93(2):209–17.

[50] Al-Allaf MH, Weekes L, Augusthus-Nelson L. Experimental study on bond-slip behaviour between CFRP sheets and lightweight concrete. In: Advanced composites in construction, ACIC 2015 - Proceedings of the 7th biennial conference on advanced composites in construction. 2015, p. 122–7.

[51] Obaidat YT, Heyden S, Dahlblom O. Evaluation of parameters of bond action between FRP and concrete. J Compos Construct 2013;17(5):626–35.

[52] Bencardino F, Condello A. SRG/SRP–concrete bond–slip laws for externally strengthened RC beams. Compos Struct 2015;132:804–15.

[53] Cornetti P, Carpinteri A. Modelling the FRP-concrete delamination by means of an exponential softening law. Eng Struct 2011;33(6):1988–2001.

[54] Al-Allaf MH, Weekes L, Augusthus-Nelson L. Shear behaviour of lightweight concrete beams strengthened with CFRP composite. Mag Concr Res 2019;71(18):949–64. http://dx.doi.org/10.1680/jmacr.17.00488.

[55] Nakaba K, Kanakubo T, Furuta T, Yoshizawa H. Bond behavior between fiber-reinforced polymer laminates and concrete. Struct J 2001;98(3):359–67.

[56] Savoia M, Ferracuti B, Mazzotti C. Non linear bond-slip law for FRP-concrete interface. In: Fibre-reinforced polymer reinforcement for concrete structures: (in 2 Volumes). World Scientific; 2003, p. 163–72.